Research Paper

An immune-related prognostic signature associated with immune landscape and therapeutic responses in gastric cancer

Jian-Rong Sun[1,*], Chen-Fan Kong[2,*], Xiang-Ke Qu[1], An-Tao Sun[3], Kun-Peng Zhao[4], Jin-Hui Sun[5]

[1]School of Clinical Medicine, Beijing University of Chinese Medicine, Beijing 100029, China
[2]School of Clinical Medicine, Shanghai University of Traditional Chinese Medicine, Shanghai 201203, China
[3]Department of Hematology, Guang'anmen Hospital, Beijing 100053, China
[4]School of Traditional Chinese Medicine, Gansu University of Chinese Medicine, Lanzhou 730000, China
[5]Department of Gastroenterology, Beijing University of Chinese Medicine Affiliated Dongzhimen Hospital, Beijing 100700, China
[*]Equal contribution

Correspondence to: Jin-Hui Sun; **email:** sunjinhui@bucm.edu.cn
Keywords: gastric cancer, immune-related signature, prognosis, immune infiltration, immunotherapy
Received: August 30, 2022 **Accepted:** February 13, 2023 **Published:** February 22, 2023

ABSTRACT

Immune-related genes (IRGs) have attracted attention in recent years as therapeutic targets in various tumors. However, the role of IRGs in gastric cancer (GC) has not been clearly elucidated. This study presents a comprehensive analysis exploring the clinical, molecular, immune, and drug response features characterizing the IRGs in GC. Data were acquired from the TCGA and GEO databases. The Cox regression analyses were performed to develop a prognostic risk signature. The genetic variants, immune infiltration, and drug responses associated with the risk signature were explored using bioinformatics methods. Lastly, the expression of the IRS was verified by qRT-PCR in cell lines. In this manner, an immune-related signature (IRS) was established based on 8 IRGs. According to the IRS, patients were divided into the low-risk group (LRG) and high-risk group (HRG). Compared with the HRG, the LRG was characterized by a better prognosis, high genomic instability, more CD8+ T cell infiltration, greater sensitivity to chemotherapeutic drugs, and greater likelihood of benefiting from the immunotherapy. Moreover, the expression result showed good consistency between the qRT-PCR and TCGA cohort. Our findings provide insights into the specific clinical and immune features underlying the IRS, which may be important for patient treatment.

INTRODUCTION

Gastric cancer (GC) is the fifth most common malignancy, with 1,089,103 new cases and 768,793 new deaths being reported globally in 2020 alone [1]. Due to the insidious onset of GC and lack of overt early symptoms, most patients are already in the advanced stage at the time of diagnosis, resulting in missed opportunities for surgical resection. Despite the fact that development of treatment approaches for advanced GC has seen much improvement in recent years, the 5-year survival rate of <20% is still clearly unsatisfactory [2]. In addition, the high degree of heterogeneity of GC leads to vastly different prognoses and therapeutic responses. Thus, there is an urgent need to develop prognostic signatures to predict outcomes and guide individualized treatments.

The tumor microenvironment (TME) comprises tumor cells, resident and recruited host cells (cancer-related stromal cells and immune cells), and secreted products of these cells (such as cytokines), which is closely related to the occurrence and progression of tumors [3]. Accumulating evidence suggests that, among the various cell types in the TME, the abundance and type of

tumor-infiltrating immune cells significantly influences the outcome of immunotherapy and tumor progression. For instance, high infiltration of T cells is associated with better immune checkpoint inhibitor (ICI) efficacy [4]. The CD8+ Foxp3+ T lymphocyte infiltration is increased with tumor progression as reflected by TNM stage, indicating their important role in GC progression [5]. Thus, the systematic investigation of immune phenotypes within the GC microenvironment represents a promising approach for better understanding the complex antitumor response and to guide effective immunotherapies. Several studies have reported immune-related signatures (IRS) in GC, some of them have explored the prognosis of GC patients by establishing immune-related prognostic models, others have further explored the tumor microenvironment, and still others have performed similar analyses on restricted populations only [6–9]. It is well known that immunotherapy is one of the mainstream modalities in oncology treatment today, but it remains a challenge to differentiate patients with potential immunotherapy response before treatment initiation. The studies on the immunotherapy response and chemotherapy sensitivity in GC have largely not been reported.

In the present study, we aimed to identify and validate a novel immune-related signature and a matching nomogram that can be utilized for predicting prognosis. This prognostic signature was conducive to the identification of immune infiltrating cells in the TME and assessment of immunotherapeutic response. Moreover, this immune-related signature was used for computing the IC50 of chemotherapeutic agents to predict the drug sensitivity.

MATERIALS AND METHODS

A flowchart of this study presented in Figure 1.

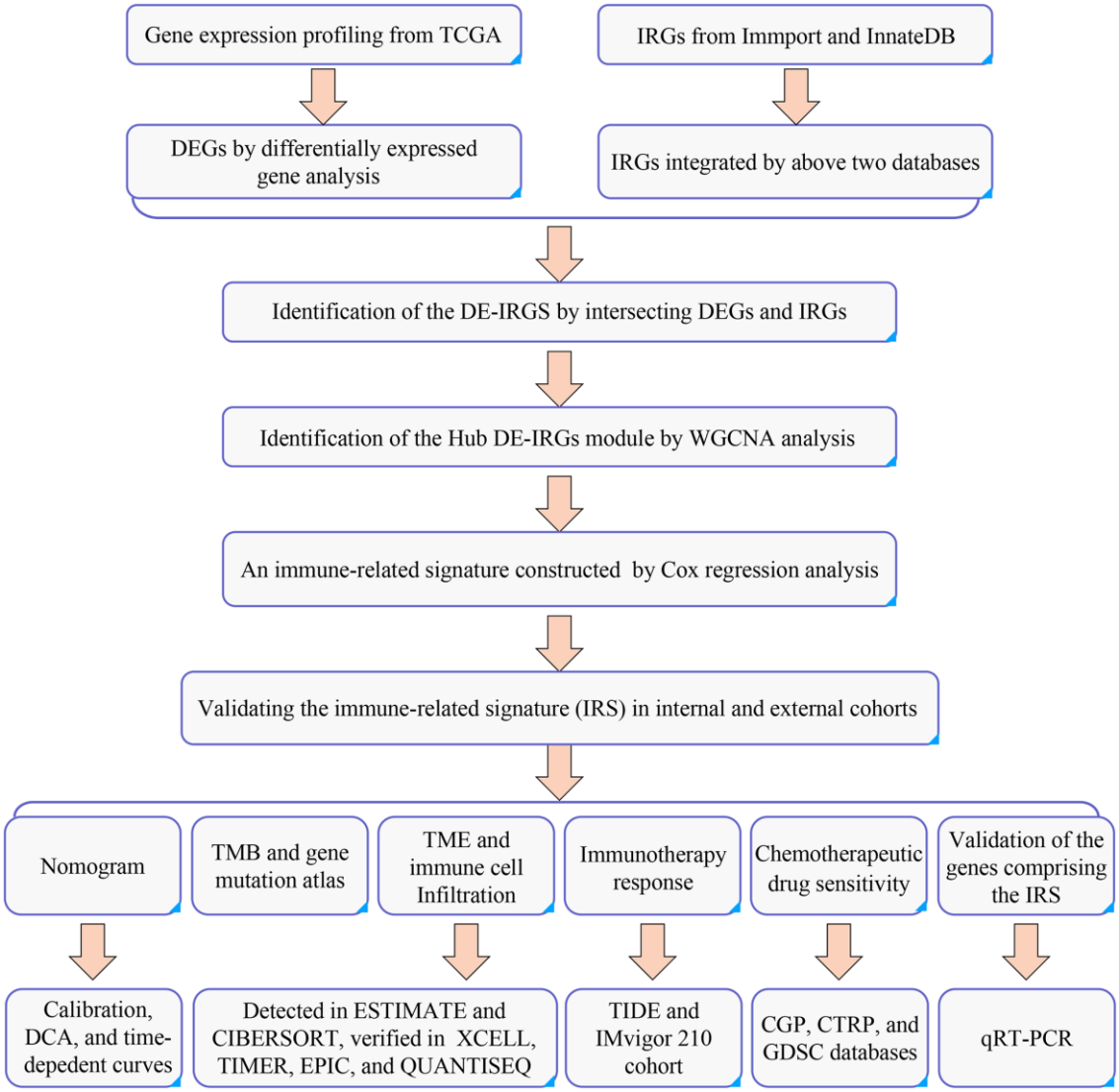

Figure 1. The flowchart of the current study.

Data acquisition

The transcriptional expression data, somatic mutation patterns, and matching clinical information (including survival time, vital status, age, gender, tumor grade, and pathological stage) of GC patients were obtained from the Cancer Genome Atlas (TCGA, https://portal.gdc.cancer.gov) database (Supplementary Table 1). An independent external GC cohort GSE84437 containing microarray data and corresponding clinical information was downloaded from the Gene Expression Omnibus (GEO, https://www.ncbi.nlm.nih.gov/geo/) database as well (Supplementary Table 1). The gene expression profile and the detailed clinical annotations of an immunotherapy cohort (IMvigor210) were acquired online (http://research-pub.gene.com/IMvigor210CoreBiologies) and utilized to further validate the efficiency of the immune-related signature (Supplementary Table 2). The immune-related gene list was obtained from the ImmPort (https://www.immport.org) and InnateDB (https://www.innatedb.ca) databases (Supplementary Tables 3, 4). As all data were obtained from public databases, ethical approval was not necessary.

Data processing

For transcriptional expression data from the TCGA database, FPKM data were transformed into TPM (transcripts per kilobase of exon model per million mapped reads) values which is more similar to microarray data, to make them more comparable between different samples [10]. The mRNA Ensembl IDs in the TCGA dataset were switched to gene symbols according to GENCODE (https://www.gencodegenes.org/). For microarray data in GEO, the probe ID in the gene expression dataset was annotated to a gene symbol by platform files (GPL6947 Illumina HumanHT-12 V3.0 expression beadchip). Next, the above datasets were normalized by log2 transformation, and the batch effects were adjusted using the ComBat function in the R3.7.0 software "sva" package [11]. mRNAs with gene expression values of 0 in >90% samples both in TCGA and GEO datasets were excluded, as they were regarded as transcriptional noise. Averaging was performed for mRNAs with more than one-row expression values.

Differentially expressed gene analysis (DEGA), differentially expressed IRG (DE-IRG) screening and functional enrichment analysis

The R "limma" package was used for identifying differentially expressed genes (DEGs) between the adjacent normal and GC samples. Those with |logFC| > 1 and FDR < 0.05 were regarded as DEGs. Next, the DEGs and IRGs were intersected to obtain DE-IRGs, and a heatmap was used to visualize the gene expression profiles of DEGs and DE-IRGs respectively by R "pheatmap" package.

GO and KEGG enrichment analysis of DE-IRGs

Gene ontology (GO) and Kyoto Genome Encyclopedia (KEGG) enrichment analyses were conducted for the DE-IRGs via the R "ClusterProfiler" package to detect their underlying biological function. The GO terms and KEGG pathways with $P < 0.05$ were regarded as significant. The above results were visualized by R "ggplot2" and "enrichplot" packages eventually.

Weighted gene co-expression network analysis (WGCNA) of DE-IRGs

WGCNA is a method for exploring gene expression patterns of multiple samples [12]. Genes with similar expression patterns can be clustered, and the relationship between modules and specific traits or phenotypes can be analyzed. Firstly, Pearson's correlation matrix was defined based on the interaction coefficients among genes. An adjacency matrix was defined with the threshold of Pearson coefficient exceeding 0.8, which was further used to construct a topological overlap matrix (TOM). Finally, the TOM matrix was applied for determining the co-expression gene modules, in this process modules with statistical significance ($P < 0.05$) were regarded as cancer-related modules, and genes involved in the modules were considered more important and used for subsequent analysis.

Identification of the immune-related signature (IRS)

In the discovery (TCGA) cohort, univariate Cox regression analysis was first conducted to detect the relationship between IRGs and GC prognosis. IRGs with $P < 0.05$ were regarded as having the potential to build the final prognostic signature. Next, to enhance the robustness of this final prognostic signature, the TCGA cohort was randomly divided into training and test subsets at a ratio of 5 to 5. In train subsets, IRGs with $P < 0.05$ in univariate Cox regression analysis were selected for inclusion in multivariate Cox regression analysis to establish the optimal prognostic signature. Particularly, the robustness of the prognostic signature was validated in the internal cohort (test cohort) and external cohort (validation cohort, GSE84437).

According to the prognostic signature, each patient was given a risk score by the following formula:

$$Risk\ Score = \sum_{k=1}^{n} Coef_k \times B_k$$

Where $Coef_k$ is the coefficient and B_K is the normalized expression value of the IRGs included in the prognostic signature. GC patients were assigned to a low-risk group (LRG) or a high-risk group (HRG) according to the cohort-specific median risk score taken as the cut-off value. The performance of risk groups as determined by the risk score of the prognostic signature was evaluated by the Kaplan-Meier method with log-rank testing. Moreover, The ROC curves at 1, 3, and 5 years were plotted and AUC values were computed to estimate the predictive performance of the signature.

In addition, we divided patients into subgroups according to clinical characteristics such as age, pathological stage, etc. We then performed stratified survival analysis to study whether the IRS maintained predictive power in different cohorts.

Development and validation of a combined IRG-clinical nomogram

A nomogram is a statistical predictive tool that combines multiple prognostic factors to assess the survival probability for individual patients. To investigate whether the IRG prognostic signature possesses independent predictive capacity. First, risk scores together with clinical parameters including age, gender, tumor grade, and pathological stage were investigated by univariate Cox regression analysis to filter prognostic factors in the TCGA cohort. The above variables with $P < 0.05$ were then selected for inclusion in multivariate Cox regression analysis to determine independent prognostic ability. A combined prognostic model consisting of factors with $P < 0.05$ in multivariate Cox regression analysis was compared with the clinical model or IRS model respectively with regard to time-dependent AUC value and calibration curve. Finally, the model was visualized by nomogram and assessed by DCA to detect whether using this nomogram could yield closer associations with clinical net-benefit than other models.

Gene functions, tumor mutation burden, and somatic mutation profiling in the different risk subgroups

Gene set enrichment analysis (GSEA) is used to evaluate the distribution trend of genes in a predefined gene set in a gene table ranked by their relevance to phenotype, thereby judging their contribution to the phenotype [13]. The functional enrichment of genes in different risk subgroups was investigated in GSEA via the R "clusterProfiler" package. The somatic mutation characteristics of GC in the LRG and HRG were analyzed and visualized using the R "maftool" package. Moreover, the tumor mutation burden (TMB) for each patient was computed as mutations per million bases.

Correlations between different risk subgroups, TME and immune cell infiltration pattern

The ESTIMATE algorithm is a tool using expression data for the estimation of stromal cells and infiltrating immune cells in malignant tumors to predict tumor purity [14]. Therefore, utilizing ESTIMATE generates three scores: a stromal score (that captures the presence of stroma in tumor tissue), an immune score (that represents the infiltration of immune cells in tumor tissue), and the estimate score (that infers tumor purity) to evaluate the main cell types in the TME. Additionally, CIBERSORT, a deconvolution algorithm supported by R package with default parameters utilizing gene expression profiles to quantify immune infiltration, was used for evaluating the proportions of 22 immune cell types in each GC tumor tissue [15]. As CIBERSORT computes an empirical *P*-value for the deconvolution to denote the accuracy of results, we only retained those samples with a CIBERSORT *P*-value < 0.05 for subsequent analysis. Furthermore, to verify the results of CIBERSORT, other algorithms such as XCELL, TIMER, EPIC, and QUANTISEQ were used for analyzing the tumor infiltration immune cells as well [16–19].

Also, based on the single sample gene set enrichment analysis (ssGSEA) method supported by the R "GSVA" package, the 29 common immune-associated pathways for each sample were given an enrichment score to quantify this. Furthermore, immune cell abundance and their corresponding functional pathways were compared in different risk groups. Finally, survival analysis was performed for immune cells and immune functions respectively to comprehensively explore the relationship between immune infiltration and GC prognosis. The macrophages could play diverse roles in tumorigenesis and progression, such as M1 macrophages (prone to anti-tumor) and M2 macrophages (pro-tumor). Thus, the expression of markers for M0, M1, and M2 macrophages were analyzed in different risk groups. Besides, expression of immune checkpoint molecules PD-1, PD-L1, and CTLA4 in different risk groups were also analyzed. Moreover, due to the cytokine and chemokine are key factors for immune cell recruitment and functions, the expression of them in the risk model was analyzed as well.

The immunotherapy response and chemotherapeutic drug sensitivity in distinct risk subgroups

The tumor immune dysfunction and exclusion (TIDE) score calculated online (http://tide.dfci.harvard.edu/)

was used to predict the immunotherapy response, the higher the TIDE score, the lower immunotherapy response [20]. Moreover, the IMvigor210 cohort was utilized to further verify the efficiency of the IRS in appraising immunotherapy responsiveness.

Based on the three public drug sensitivity databases, CGP (Cancer Genome Project), GDSC (Genomics of Drug Sensitivity in Cancer), and CTRP (Cancer Therapeutics Response Portal), the ridge regression models were built by the pRRophetic algorithm to predict chemotherapeutic responses. Gene expression profiling and risk grouping information were used in the model to estimate the half-maximal inhibitory concentrations (IC50) for each sample [21]. The prediction accuracy was evaluated by 10-fold cross-validation based on each training set. The smaller the IC50 value of the drug, the stronger its ability to inhibit cell growth and the better the effect of cancer treatment. Here, common GC therapeutic drugs, such as cisplatin, oxaliplatin, docetaxel, paclitaxel, 5-fluorouracil (5-Fu), capecitabine, and irinotecan were selected for analysis.

Immunohistochemical analysis

The protein expression data were acquired from the Human Protein Atlas (HPA) database, a largest and most comprehensive database for evaluating protein distribution in human tissues [22]. The protein expression of the IRGs signature in normal and GC tissues was determined using the immunohistochemical staining images, and then Image J was used to perform the quantitative analysis.

Validation of the immune-related signature by relative quantitative real-time PCR (qRT-PCR)

The expression levels of genes comprising the immune-relative signature were measured in a GC cell line (HGC-27, human gastric cancer cells) and a control cell line (GES-1, human gastric mucosal epithelial cells). All the cell lines were obtained from the National Infrastructure of Cell Line Resources (Beijing, China) and were in RPMI-1640 (FBS, Gibco, USA), 10% fetal bovine serum (FBS, Gibco, USA), and 1% penicillin/streptomycin (Gibco, Canada). All the cells were cultured at 37°C with 5% CO2. Total RNA was extracted from cells using the RNeasy Mini Kit (Qiagen, USA, Cat. 74104), and reverse transcription was subsequently performed using the 5∗All-in-one RT MasterMix (ABM, USA, Cat. No. G492). qRT-PCR was performed with a SYBR Green Real-time PCR Kit (Keygen Biotech, Nanjing, China, Cat. KGA1339-1) on a QuantStudio 5 Real-Time PCR System (Thermo Fisher Scientific, USA). All experiments were repeated at least three times. The RNA primer sequences are listed in Supplementary Table 5. Relative expression was calculated using the comparative threshold cycle (Ct) method. Simultaneously, the gene expression consisting of the signature was analyzed in the TCGA cohort.

Statistical analysis

All statistical analyses were conducted via R software (version 3.7.0). Continuous and categorical data were analyzed by Wilcoxon and Chi-square methods respectively. Survival was estimated by the Kaplan-Meier method and the statistical significance was determined by log-rank testing. Correlations between two continuous characteristics were analyzed by the Spearman method. Univariate and multivariate Cox regression analyses were performed using the R "survival" package. The time-dependent AUC value was calculated by the R "timeROC" package, and ROC curves were plotted by R "survivalROC" package. $P < 0.05$ was regarded as statistically significant.

Data availability statement

The data that support this study are openly available in online repositories and the raw data was uploaded (https://www.jianguoyun.com/c/sd/155e27d/6d60f576ace1d1cc).

RESULTS

Identification of DE-IRGs and functional enrichment analysis

With the cut-off set as logFC > 1, FDR < 0.05, there were 8833 DEGs identified totally, of which 1335 were down-regulated and 7498 were up-regulated (Supplementary Table 6). By searching ImmPort and InnateDB, 2483 and 1226 IRGs (Supplementary Tables 7, 8) were determined separately as well as 2660 IRGs were obtained by integrating IRGs from the two databases (Supplementary Table 9). Next, overlaps of DEGs and IRGs identified 493 DE-IRGs, comprising 184 that were down-regulated and 309 up-regulated (Supplementary Table 10). As shown in Figure 2A, 2B, there was a clear distinction of DEGs and DE-IRGs between normal and tumor samples.

These 493 DE-IRGs were further analyzed via GO and KEGG to explore their function. In GO enrichment analysis, the biological process (BP) term showed that these DE-IRGs were enriched in leukocyte migration, regulation of the inflammatory response, cell chemotaxis, regulation of immune effector processes, and regulation of responses to external stimuli.

The cellular component (CC) terms showed that these DE-IRGs were mainly enriched for the immunoglobulin complex, external side of plasma membrane, and collagen-containing extracellular matrix. Concerning molecular function (MF), these DE-IRGs were enriched in terms of receptor-ligand activity, cytokine activity, cytokine receptor binding, and growth factor activity (Figure 2C). Moreover, KEGG pathway analysis documented that these DE-IRGs were principally enriched in cytokine-cytokine receptor interaction, neuroactive ligand-receptor interaction, chemokine signaling pathway, viral protein interaction with cytokine and cytokine receptor, cAMP signaling pathway, and MAPK signaling pathways (Figure 2D).

Detecting hub DE-IRGs via WGCNA analysis

DE-IRGs were further selected for WGCNA analysis to distinguish different gene modules and then to identify the hub DE-IRGs. A soft threshold (power value) of 5 was selected to make sure that both the scale-free topology model fit index (R^2) and mean connectivity

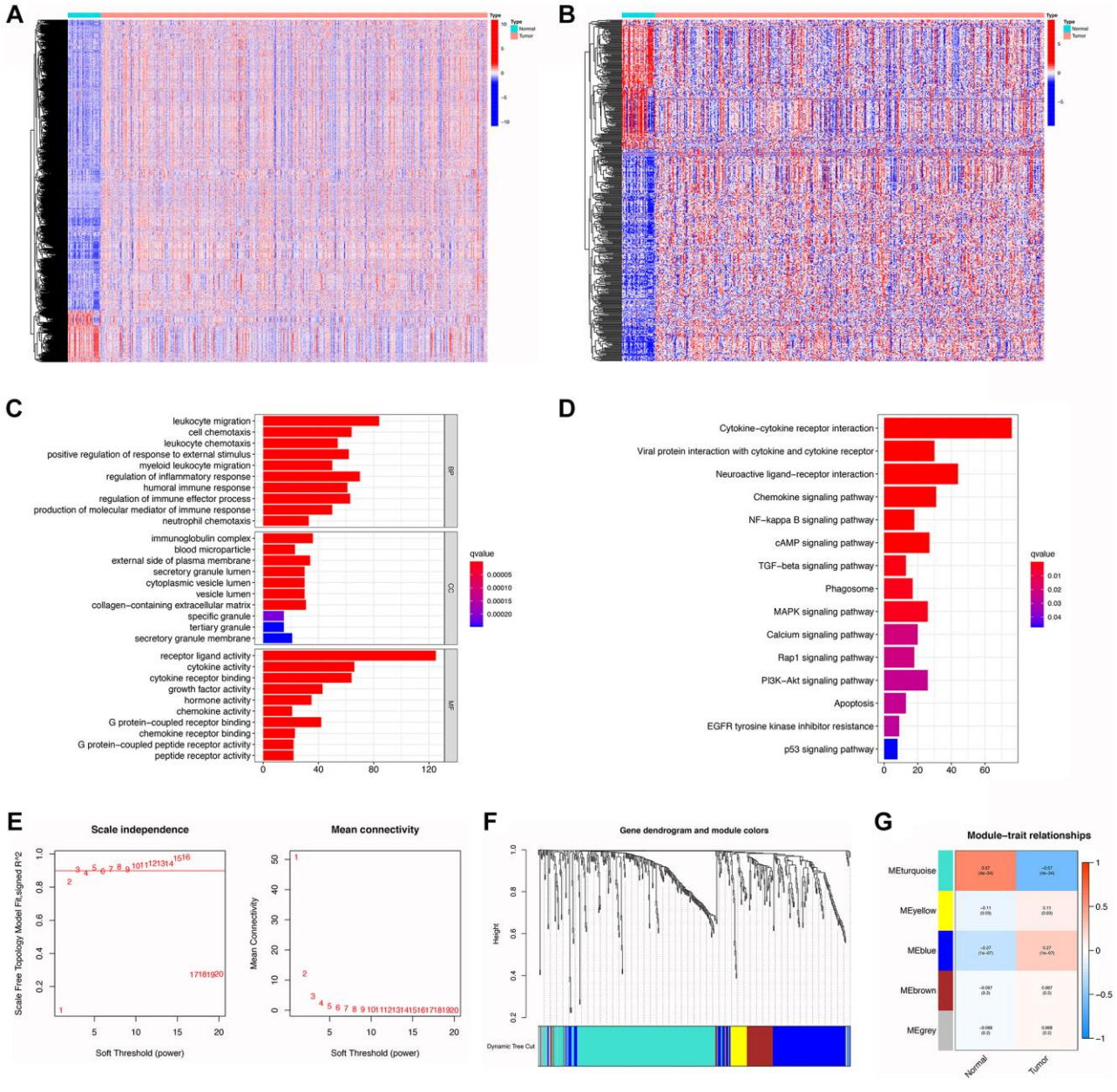

Figure 2. Identification, functional enrichment, and WGCNA analysis of DE-IRGs. (**A**, **B**) Heatmap of DEGs and DE-IRGs, respectively. (**C**, **D**) GO enrichment and KEGG analysis for DE-IRGs. (**E**) The scale-free fit index for soft-thresholding powers. Left: the relationship between the soft-threshold and scale-free R2. Right: the relationship between the soft-threshold and mean connectivity. (**F**) Dendrogram and module colors for DE-IRGs. (**G**) The correlations heatmap between modules and sample types.

were optimal (Figure 2E). A total of 5 modules was obtained by average linkage hierarchical clustering. Each module is shown in a different color in Figure 2F. Among these modules, MEturquoise possessed the highest correlation with GC traits (Figure 2G). There were 255 DE-IRGs included in the filtered MEturquoise module, which were chosen for further analysis (Supplementary Table 11).

Construction and verification of the immune-related prognostic signature

Utilizing univariate Cox regression analysis, a total of 36 genes was identified as being associated with GC prognosis (Figure 3A). We then constructed an 8-gene signature by multivariate Cox regression analysis in the training subset (Supplementary Table 12). The risk scores for each GC patients were calculated as follows:

Risk Score = (0.277) × *RNASE2* + (0.255) × *CGB5* + (0.501) × *INGBE* + (−0.348) × *PTGER3* + (−0.341) × *CTLA4* + (0.260) × *DUSP1* + (0.071) × *APOA1* + (0.234) × *CD36*.

Next, all GC patients were assigned to either a lower or higher risk group: LRG (n = 93) and HRG (n = 93). The results of Kaplan-Meier analysis and log-rank testing showed that patients in the LRG had a better overall survival rate (OS) than the HRG (Figure 3B). The AUC values of ROC curves for predicting survival outcomes at 1, 3, 5 years were 0.69, 0.86, and 0.87, respectively, demonstrating that the signature possesses good predictive capacity for GC prognosis (Figure 3C). In addition, the results of IRS validation showed that this signature maintain its prognosis predictive power in test subsets and validation cohorts as well (Figure 3D–3G).

Furthermore, we conducted stratified analysis for the IRS based on clinical characteristics such as age, gender, tumor grade, and pathological stage to explore the signature's robustness. The results showed that patients in the HRG generally have a poor prognosis in different sub-cohorts compared with the LRG, which is consistent with the result from the integrated cohort. This confirms the robustness of this IRS in cohorts with different clinical features (Table 1).

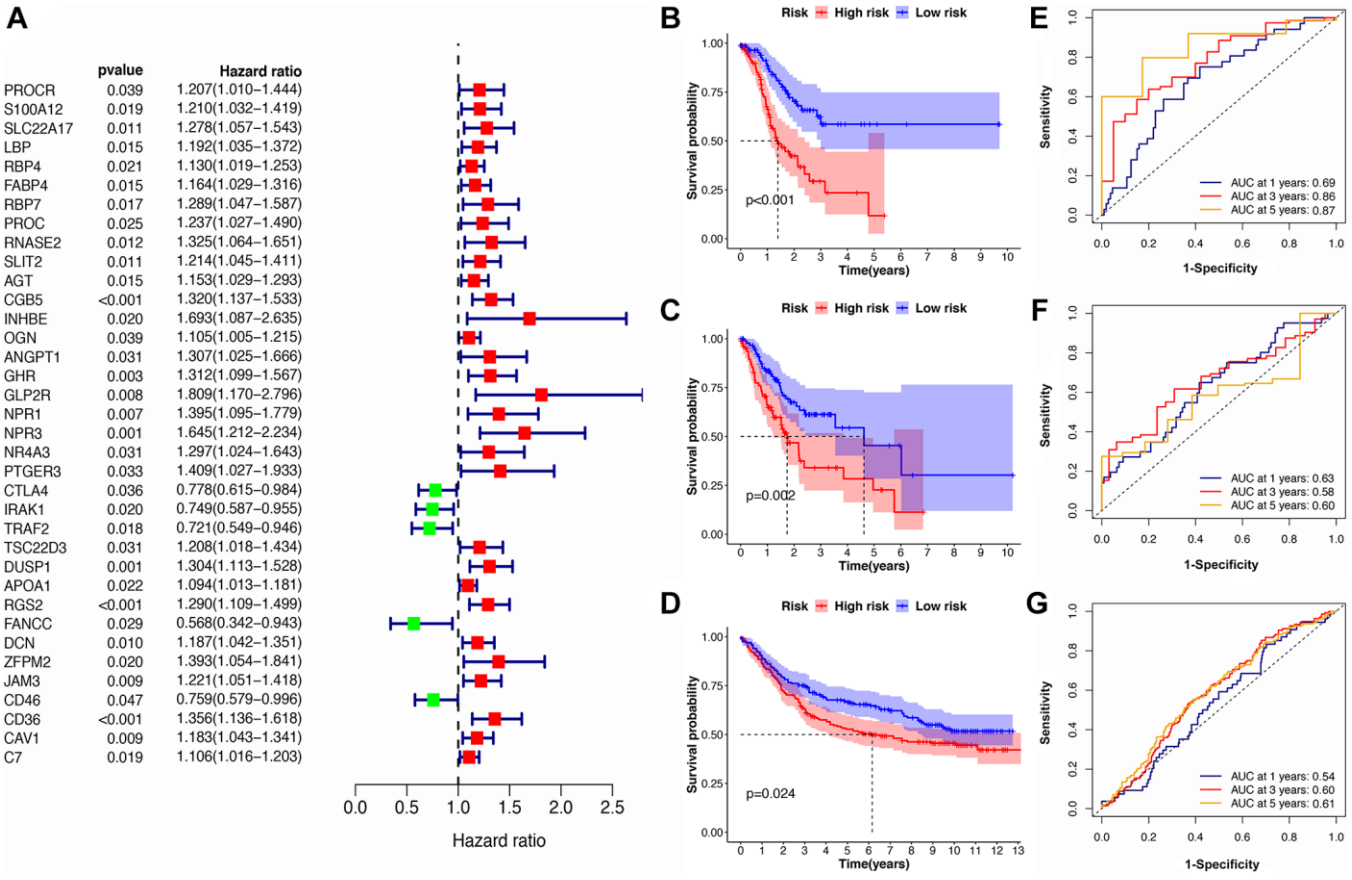

Figure 3. Identification of the immune-related prognostic signature. (**A**) The forest plot of univariate Cox regression analysis for IRGs. (**B–D**) The Kaplan-Meier survival curves for high- and low-risk groups in train, test, and validation cohorts. (**E–G**) The ROC curve for the IRS in train, test, and validation cohorts.

Table 1. Cox survival analysis of the IRS in stratified GC cohort.

Variables	TCGA-STAD				GSE84437	
	Training cohort		Test cohort			
	HR (95% CI)	*P* value	HR (95% CI)	*P* value	HR (95% CI)	*P* value
Age (years)						
≤65	6.46 (2.16–19.31)	<0.001	2.52 (1.13–5.65)	0.025	1.60 (1.01–2.56)	0.047
>65	2.22 (1.19–4.13)	0.012	1.88 (1.03–3.45)	0.040	1.36 (0.88–2.11)	0.170
Gender						
Male	3.19 (1.69–6.02)	<0.001	1.55 (0.85–2.82)	0.150	1.30 (0.94–1.80)	0.107
Female	2.76 (1.05–7.34)	0.040	3.13 (1.38–7.09)	0.006	1.71 (1.07–2.98)	0.036
Tumor grade						
G1/2	2.50 (0.98–6.37)	0.054	1.37 (0.61–3.06)	0.448	—	—
G3/4	2.61 (1.33–5.12)	0.005	2.41 (1.32–4.43)	0.004	—	—
Pathological stage						
Stage I/II	3.20 (1.22–8.36)	0.018	2.03 (1.78–4.63)	0.018	1.65 (1.31–2.65)	0.025
Stage III/IV	2.93 (1.55–5.55)	<0.001	2.02 (1.11–3.69)	0.021	1.83 (1.07–2.69)	0.015
T stage						
T1/2	2.94 (0.73–11.86)	0.130	2.87 (0.91–9.12)	0.073	0.49 (0.12–2.00)	0.326
T3/4	3.27 (1.82–5.87)	<0.001	1.99 (1.17–3.39)	0.011	1.40 (1.06–1.86)	0.019
N stage						
N0	4.32 (1.32–14.18)	0.016	2.39 (1.35–6.69)	0.027	1.98 (1.45–2.14)	0.017
N1–3	2.86 (1.53–5.34)	<0.001	1.86 (1.08–3.20)	0.025	1.37 (1.01–1.84)	0.040
M stage						
M0	3.14 (1.79–5.53)	<0.001	1.79 (1.07–2.99)	0.027	1.48 (1.04–2.11)	0.029
M1	2.45 (0.23–25.77)	0.455	2.76 (0.55–13.90)	0.218	1.21 (0.77–1.86)	0.408

The "—" indicates that the value is not available; Abbreviations: HR: hazard ratio; CI: confidence interval.

Establishment and validation of an immune-clinical nomogram

The Cox regression analysis of the discovery cohort showed that age, pathological stage, and risk score were independent prognostic factors for GC patients (Table 2). Therefore, these factors were combined to construct a nomogram for predicting GC patients' short- and long-term survival rates (Figure 4A). The time-dependent AUC value of the nomogram remained higher than for other models over time, suggesting that combining the IRS with age and pathological stage improved accuracy for predicting survival outcomes (Figure 4B). The calibration curve of the nomogram showed a good performance in consistency between prediction and actual observation, especially for 3-year OS. Also, the DCA curve suggested that the nomogram possessed better value for clinical applications than the other models (Figure 4C, 4D).

In the validation cohort, the time-independent AUC value and calibration curve of the nonogram model maintained its good performance for predicting patients' OS as well (Figure 4E, 4F). DCA revealed that utilizing the nomogram could bring more clinical net benefit (Figure 4G). Thus, the nomogram comprising IRS and clinical characteristics (pathological stage and age) appeared highly accurate in predicting the short- and long-term OS of GC patients in both the discovery and validation cohorts. The above results demonstrated that using this immune-clinical nomogram for prognosis prediction assistance might result in significant clinical benefit.

Table 2. Univariate and multivariate Cox regression analysis for clinical variables.

Variables	Univariate analysis		Multivariate analysis	
	HR (95% CI)	*P* value	HR (95% CI)	*P* value
Age				
≤65	Reference		Reference	
>65	1.03 (1.01–1.04)	0.005	1.04 (1.02–1.05)	<0.001
Gender				
Female	Reference		—	—
Male	1.23 (0.85–1.76)	0.274	—	—
Tumor grade				
G1–2	Reference		—	—
G3–4	1.33 (0.93–1.91)	0.123	—	—
Pathological stage				
Stage I/II	Reference			
Stage III/IV	1.80 (1.26–2.57)	0.001	1.76 (1.21–2.55)	0.003
T				
T1–2	Reference			
T3–4	1.63 (1.05–2.52)	0.030	1.38 (0.84–2.29)	0.207
N				
N0	Reference		Reference	
N1–3	1.74 (1.15–2.62)	0.008	1.26 (0.72–2.20)	0.415
M				
M0	Reference		Reference	
M1	1.79 (1.09–2.95)	0.022	1.45 (0.85–2.48)	0.178
Risk Score				
Low	Reference		Reference	
High	1.57 (1.37–1.80)	<0.001	1.58 (1.37–1.84)	<0.001

The '—' indicates that the value is not available; Abbreviations: HR: hazard ratio; CI: confidence interval.

GSEA analysis, TMB, and a gene mutation atlas in different risk subgroups

As shown in Figure 5A, 5B, GSEA analysis indicated that tumors in the HRG were enriched in complement and coagulation cascades, ECM receptor interaction, focal adhesion, neuroactive ligand-receptor interaction, and PPAR signaling pathway. In contrast, the LRG was enriched in aminoacyl tRNA biosynthesis, cell cycle, DNA replication, pyrimidine metabolism, and spliceosome terms.

Summaries of gene mutation profiles for the different risk groups are shown in the Supplementary Figures 1 and 2, suggesting that the LRG has a higher overall mutation frequency than the HRG. Nonetheless, the top six genes with the highest mutation rates in the LRG were *TTN* (54%), *TP53* (44%), *MUC16* (35%), *LRP1B* (28%), *ARID1A* (28%), and *SYNE1* (27%), which is similar to the HRG with *TTN* (40%), *TP53* (39%), *MUC16* (25%), *LRP1B* (20%), *ARID1A* (19%), and *SYNE1* (16%). The most common mutation type was missense mutation in both LRG and HRG (Figure 5C, 5D).

TMB analysis in the HRG and LRG is shown in Figure 5E, 5F, suggesting that the latter has a higher TMB. In addition, survival analysis of patients stratified for TMB indicated that a high TMB resulted in a better prognosis than a low TMB.

Analysis of the tumor microenvironment, immune cell infiltration, and expression of markers for macrophages, immune checkpoint, cytokine, and chemokine in different risk groups

First, the difference between the TME and immune cell infiltration was analyzed for LRG and HRG. As shown

in Figure 6A–6C, the stromal score and ESTIMATE score were both higher in HRG than LRG, whereas the immune score was not significantly different, indicating that the HRG had a higher proportion of stromal cells than LRG while tumor purity was lower.

Second, by using the CIBERSORT, the abundance of immune cells in each GC sample was estimated and can be seen intuitively in the histogram (Supplementary Figure 3). The number of samples with significant levels of immune cell infiltration in the HRG was

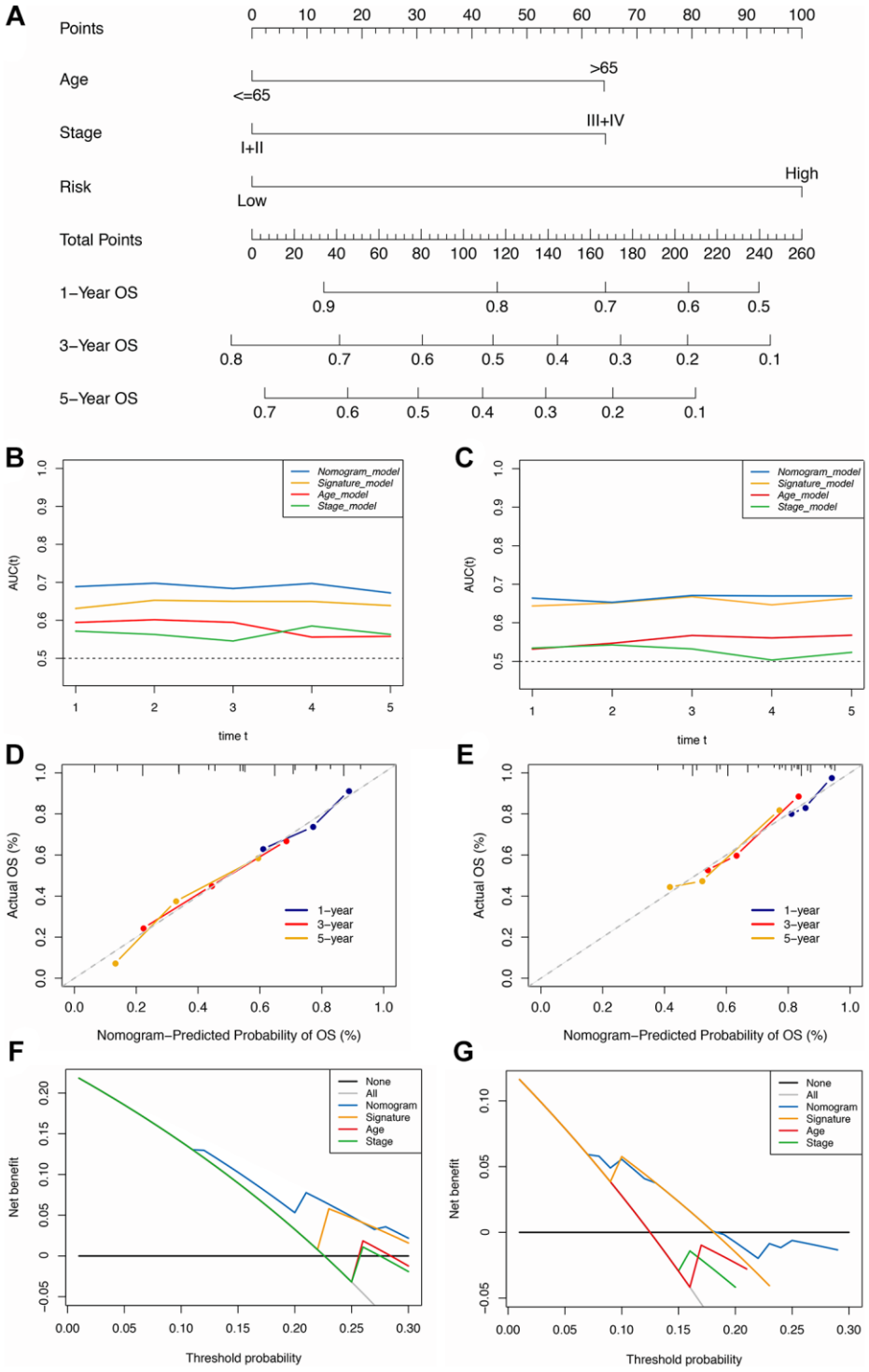

Figure 4. Construction of the immune-clinical nomogram. (**A**) The nomogram for predicting 1-year, 3-year, and 5-year OS for GC patients. (**B**, **C**) Time-dependent ROC curves for the nomogram, immune signature, age, and stage models at different time points in the TCGA and GEO datasets. (**D**, **E**) Calibration curves of observed and predicted probabilities for the nomogram in the TCGA and GEO datasets. (**F**, **G**) DCA curves for the nomogram in the TCGA and GEO datasets.

greater than in the LRG. Score difference analysis for immune cells' abundance in different risk groups showed that compared with the HRG, the LRG had higher abundances of CD8+ T cells ($P < 0.01^{**}$), CD4+ activated memory T cells ($P < 0.001^{***}$), follicular T helper cells ($P < 0.001^{***}$), and M1 macrophages ($P < 0.01^{**}$). On the other hand, there was a lower abundance of monocytes ($P < 0.001^{***}$), M2 macrophages ($P < 0.001^{***}$), eosinophils ($P < 0.05^{*}$), and neutrophils ($P < 0.001^{***}$) (Figure 6D). Notably, the results of XCELL, TIMER, EPIC, and QUANTISEQ showed good consistency with the CIBERSORT (Supplementary Figure 4). Score differences for immune-related functional pathways suggested that the scores for cytolytic activity ($P < 0.05^{*}$), inflammation promoting ($P < 0.01^{**}$), MHC class I ($P < 0.001^{***}$), T cell co-inhibition ($P < 0.05^{*}$), Th1 cells ($P < 0.05^{*}$), and Th2 cells ($P < 0.001^{***}$) were higher in LRG than in HRG. In contrast, the scores for CCR ($P < 0.01^{**}$), DCs ($P < 0.01^{**}$), iDCs ($P < 0.01^{**}$), macrophages ($P < 0.001^{***}$), mast cells ($P < 0.001^{***}$), neutrophils ($P < 0.001^{***}$), T helper cells ($P < 0.05^{*}$), and type II IFN responses ($P < 0.001^{***}$) were lower in the LRG than in the HRG (Figure 6E). Moreover, survival analysis based on immune cells' abundance in all samples implied that high infiltration of CD8+ T cells was connected with a favorable prognosis and that high abundance of M2 macrophage was related to an adverse prognosis (Figure 7A, 7B). This confirms that specific immune infiltration patterns have impact on patient prognosis. Survival analysis for immune-associated pathways suggested that high enrichment scores for cytolytic activity, inflammation promoting, T cell co-inhibition, and Th2 cell presence were associated with a favorable prognosis, whereas IDCs, mast cells, neutrophils, and type II IFN responses were associated with adverse prognosis (Figure 7C–7J).

The expression analysis for markers of macrophages indicated that the marker gene of M0 macrophages like CD68 was highly expressed in the high-risk group (Supplementary Figure 5A), CD86 for M1 macrophages was lowly expressed in the high-risk group (Supplementary Figure 5B), similarly, NOS2 tended to be down-regulated in the high-risk group (Supplementary Figure 5C). Moreover, the markers for M2 macrophages like CD163 and CD206 were highly expressed in the high-risk group (Supplementary

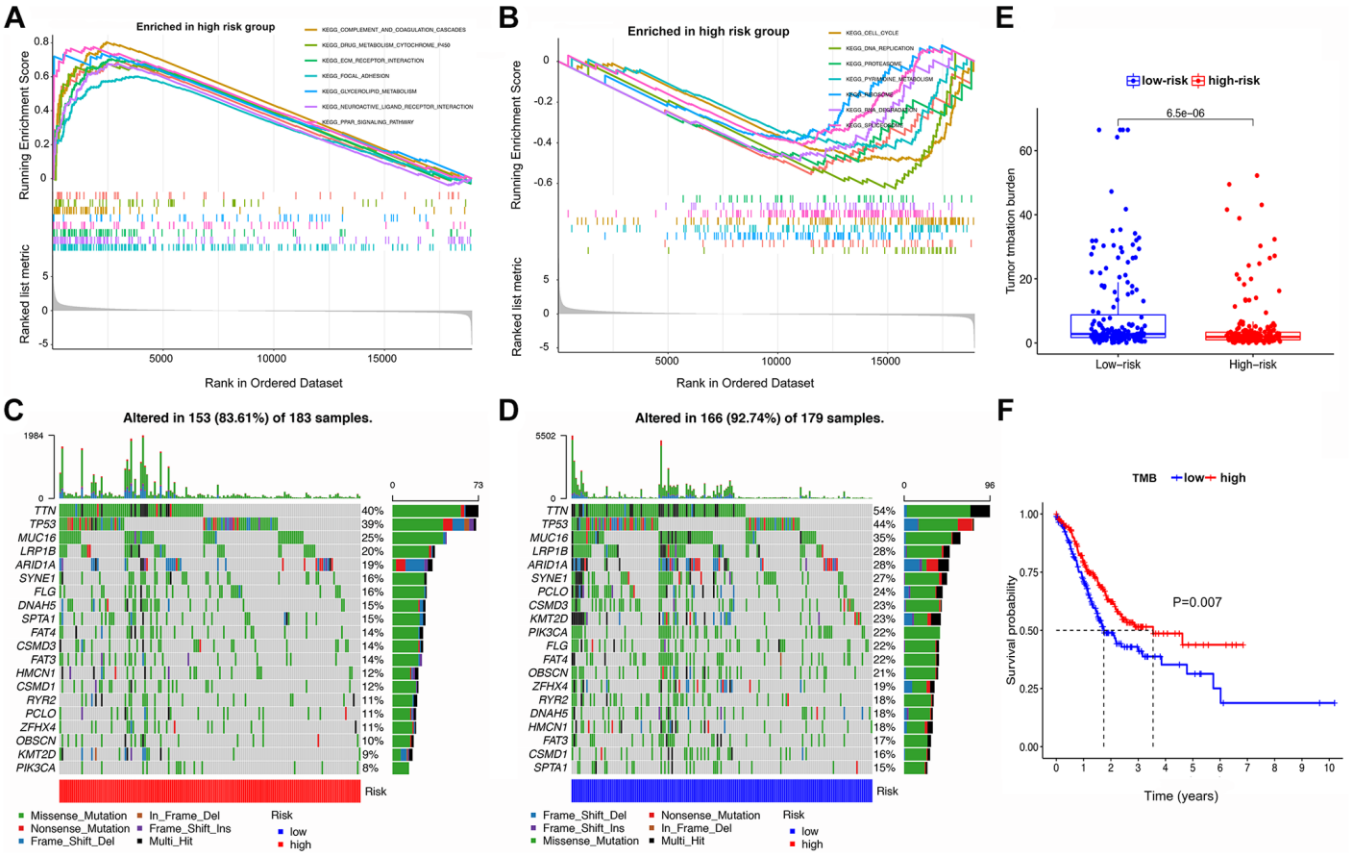

Figure 5. GSEA, mutational landscape, and TMB in high- and low-risk groups stratified by the IRS. (**A**, **B**) The enriched pathways for different risk groups based on GSEA analysis (**C**, **D**) Waterfall plot of the top 20 mutant genes in the high- and low-risk groups. (**E**) Box plot for the TMB between the high- and low-risk groups. (**F**) Kaplan-Meier survival curve of high versus low TMB.

Figure 5D, 5E). The aforesaid results were consistent with the analysis of tumor infiltration immune cells for macrophages.

Analysis of immune checkpoints showed that PD-1, PD-L1, and CTLA4 were more highly expressed in LRG than in HRG, with decreasing expression as the risk score increased (Figure 8A–8F). The results of cytokine suggested that IFN-γ, IL-21, and OSM had higher expression in LRG than in HRG while IL-1α, IL-1β, IL-10, IL-24, TGF-β, EGF, and VEGF had lower expression in LRG than in HRG (Supplementary Figure 6A–6J). The analysis of chemokine showed that CCL2, CCL7, and CXCL8 were highly expressed in the HRG than in the LRG whereas the CXCL9, CXCL10, and CXCL11 were highly expressed in the LRG than in the HRG (Supplementary Figure 6K–6P).

Immunotherapy response and chemotherapeutic drug sensitivity prediction based on the IRS to improve the GC patients' survival

Compared with the HRG, the LRG presented with lower TIDE scores, indicating that the latter may have a greater response to ICI than the former (Figure 8G–8I). In the immunotherapy cohort, patients in the LRG had a

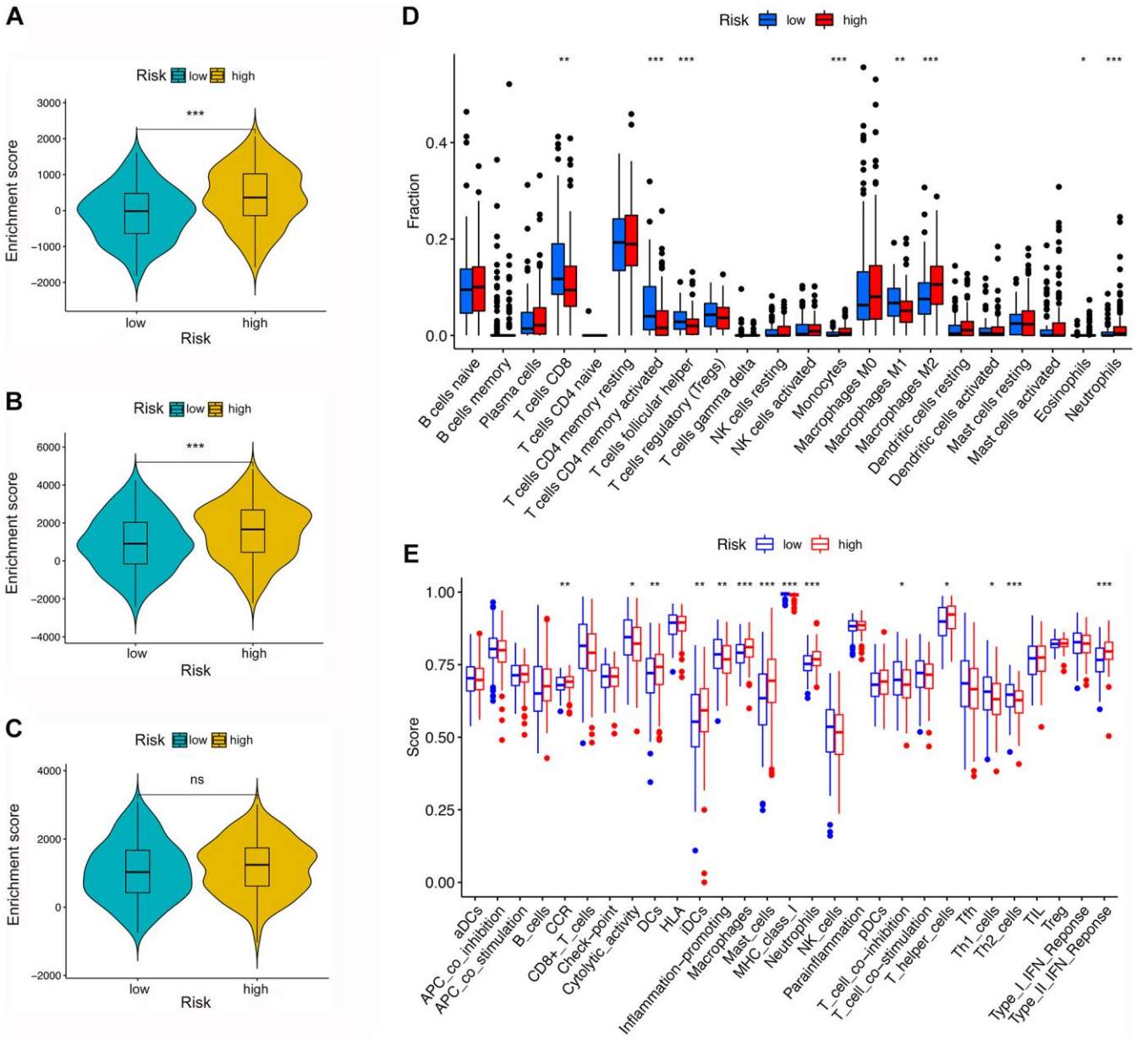

Figure 6. TME and immune cell infiltration in different risk groups. (**A**–**C**) TME analysis based on ESTIMATE algorithm. From top to bottom: The stromal score, ESTIMATE score, and immune score. (**D**) Immune cell infiltration in high- and low-risk groups based on the CIBERSORT algorithm. (**E**) Immune-related pathways based on ssGSEA.

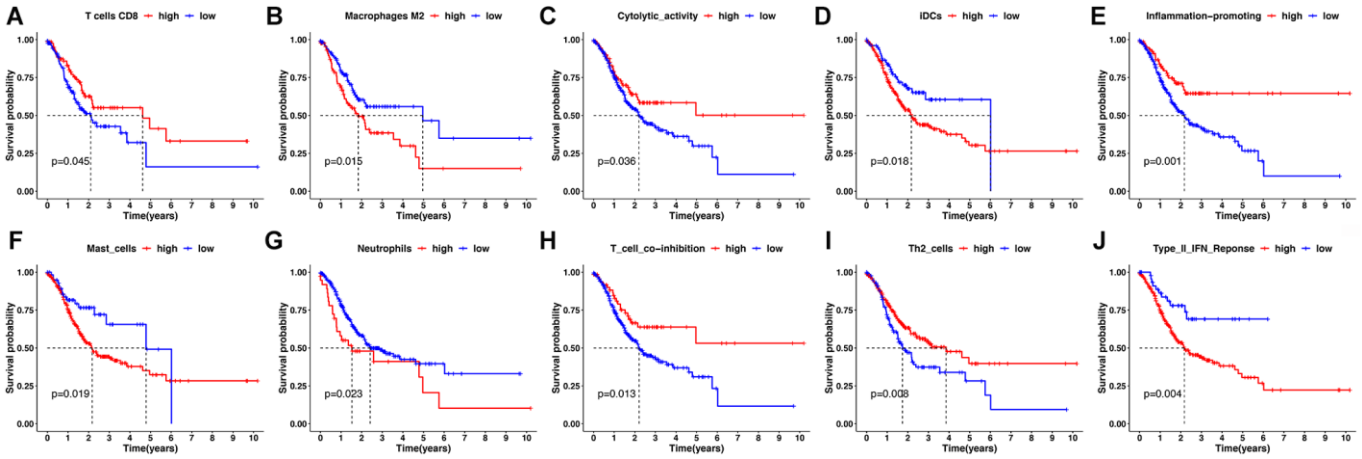

Figure 7. Kaplan-Meier survival analysis for immune infiltration cell and immune-related pathway. (**A**, **B**) Kaplan-Meier survival curves for immune infiltrating CD8+ T cells and M2 macrophages. (**C–J**) Kaplan-Meier survival curves for immune-related pathway.

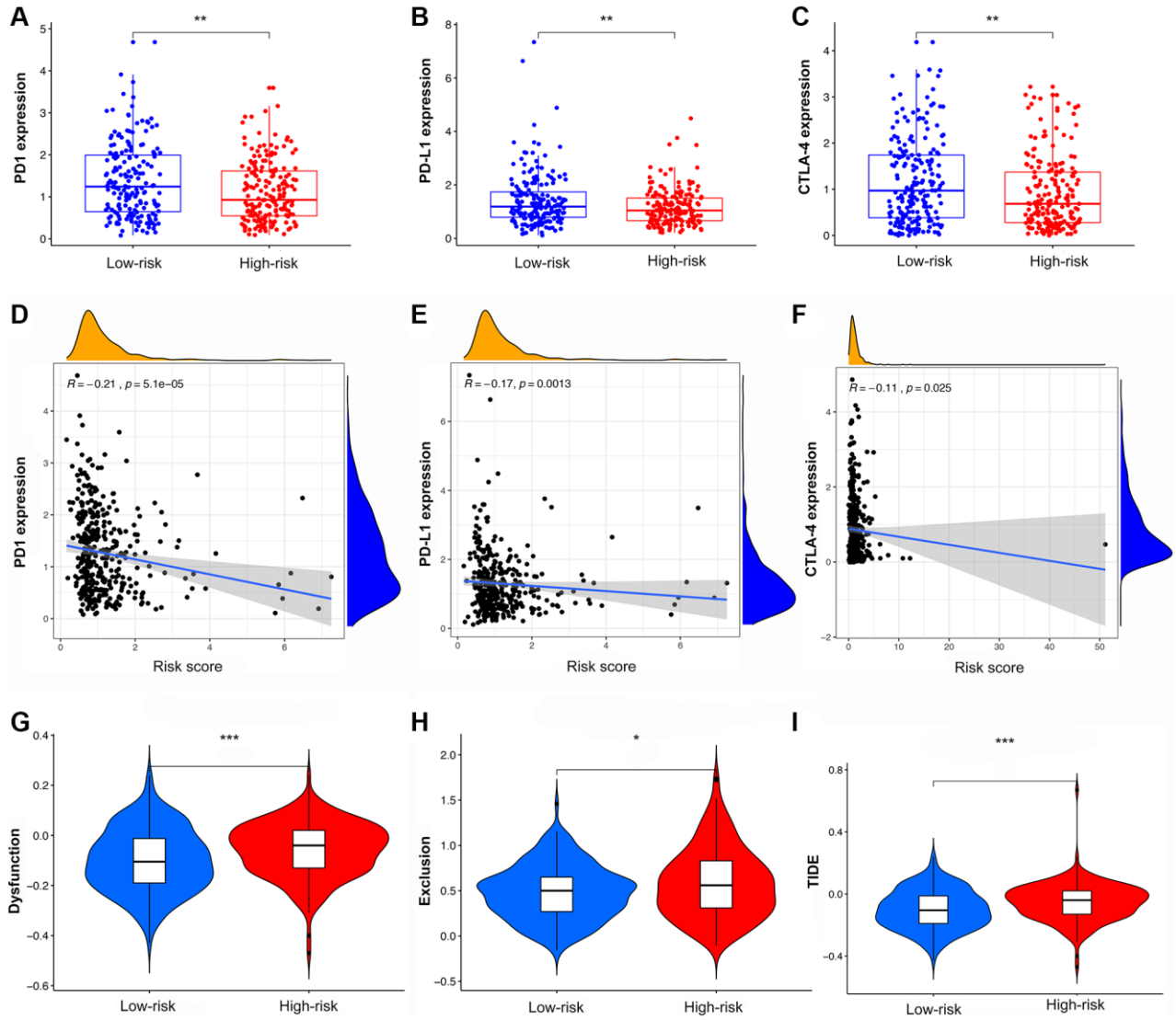

Figure 8. The analysis of TIDE score and expression of immune checkpoints in high- and low-risk groups. (**A–C**) The expression of PD1, PD-L1, and CTLA4 in different risk groups. (**D–F**) The co-expression patterns between immune checkpoints and risk scores. (**G–I**) The scores of immune dysfunction, immune exclusion, and TIDE in different risk groups.

markedly longer survival time (Figure 9A). Compared with HRG, the LRG had a better therapeutic advantage and immunotherapy response (Figure 9B). Moreover, the TMB was significantly elevated in LRG, which is closely linked to immunotherapeutic efficacy (Figure 9C). Also, the association between the IRS and survival on immunotherapy remained statistically significant after taking into account gender, smoking, ECOG score, immune phenotype, and TMB status (Figure 9D).

Three drug response-related databases (CGP, GDSC, and CTRP) were utilized to investigate the association between the chemotherapeutic drug sensitivity and the IRS. Results suggested that patients in the LRG are generally more sensitive to chemotherapeutic drugs than those in the HRG (Figure 10).

Expression of the genes in the immune-related signature

The quantitative analysis of the immunohistochemical images determined that *CD36*, *DUSP1*, and *PTGER3* showed lower protein expression levels in GC samples than in the adjacent normal tissues while *CGB5* showed

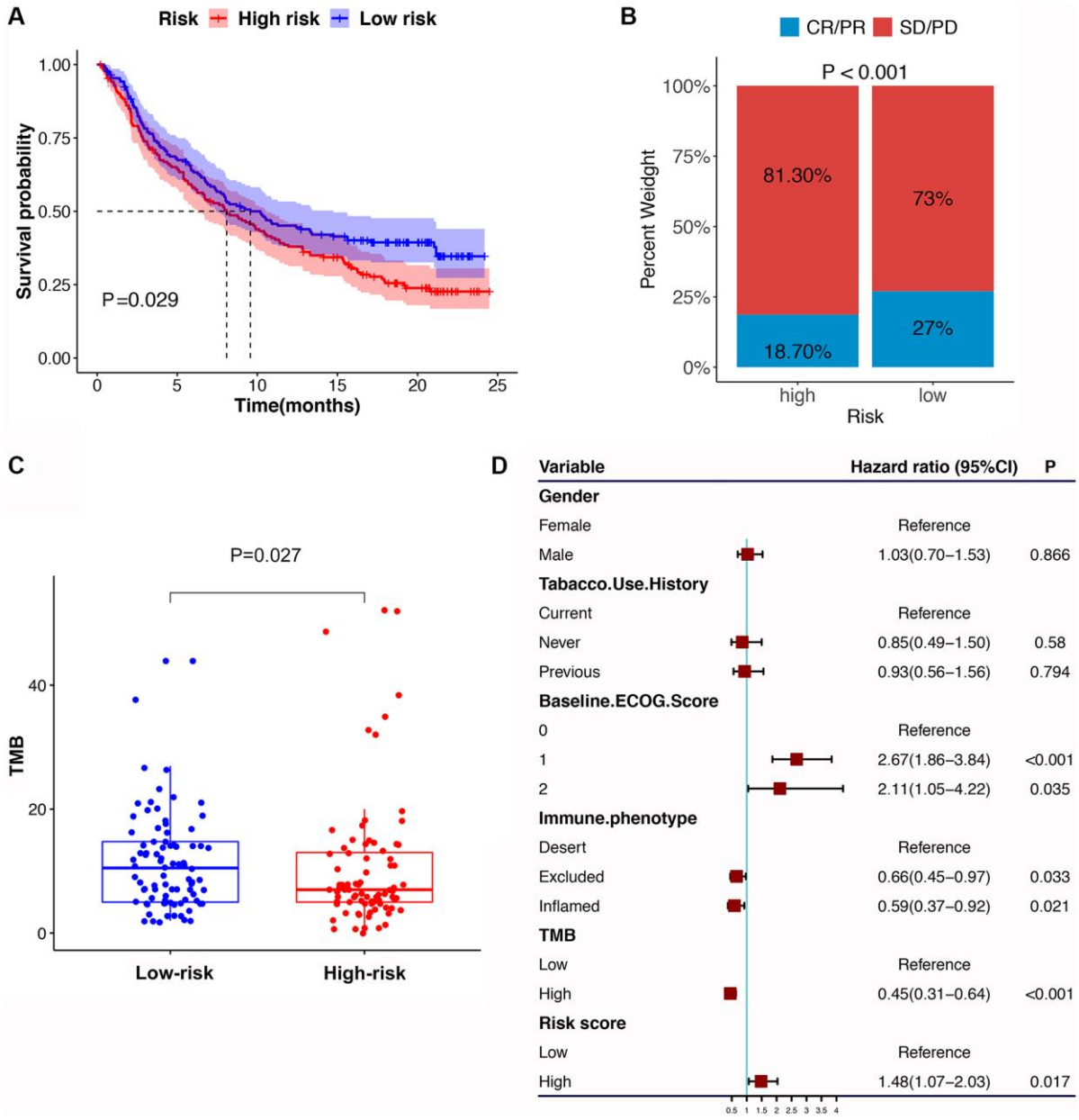

Figure 9. The IRS in the role of immune checkpoint blocker treatment. (**A**) Kaplan-Meier survival curve of the high- versus low-risk group in the immunotherapy cohort (IMvigor210 cohort). (**B**) The proportion of immune response to immunotherapy in high versus low-risk group. (**C**) The tumor mutation burden in the immunotherapy cohort was compared among distinct risk groups. (**D**) Multivariate Cox regression analysis of the IRS with features in the immunotherapy cohort.

high levels in GC samples than in the normal tissues. The expression of *APOA1*, *INHBE*, and *RNASE2* did not differ significantly in gastric cancer and normal samples, and the *CTLA4* was not reported in the database (Supplementary Figures 7, 8).

Validation of the immune-related signature by qRT-PCR

The expression profiles of the eight genes comprising the prognostic signature were verified in GC and stomach cell lines by qRT-PCR. The result suggested that *RNASE2*, *INHBE*, *CGB5*, and *CTLA4* were upregulated in GC cell lines, while *PTGER2*, *DUSP1*, *CD36*, and *APOA1* were downregulated (Figure 11A), which showed good consistency with the expression analysis results in TCGA cohort (Figure 11B).

DISCUSSION

In the current study, we identified the IRGs that were significantly correlated with the prognosis of GC patients. We then constructed an IRS to predict the prognosis of patients assigned to the different risk groups. This signature was combined with clinical characteristics to build a composite nomogram, which exhibited an accurate prediction capacity for GC patients' prognosis. Finally, we investigated the relationship between the IRS and the somatic mutation, pathway activation, immune cell infiltration, immunotherapy responsiveness, and chemotherapeutic drug sensitivity.

GC is a highly heterogeneous malignant tumor with a poor prognosis. The traditional TNM classification is a

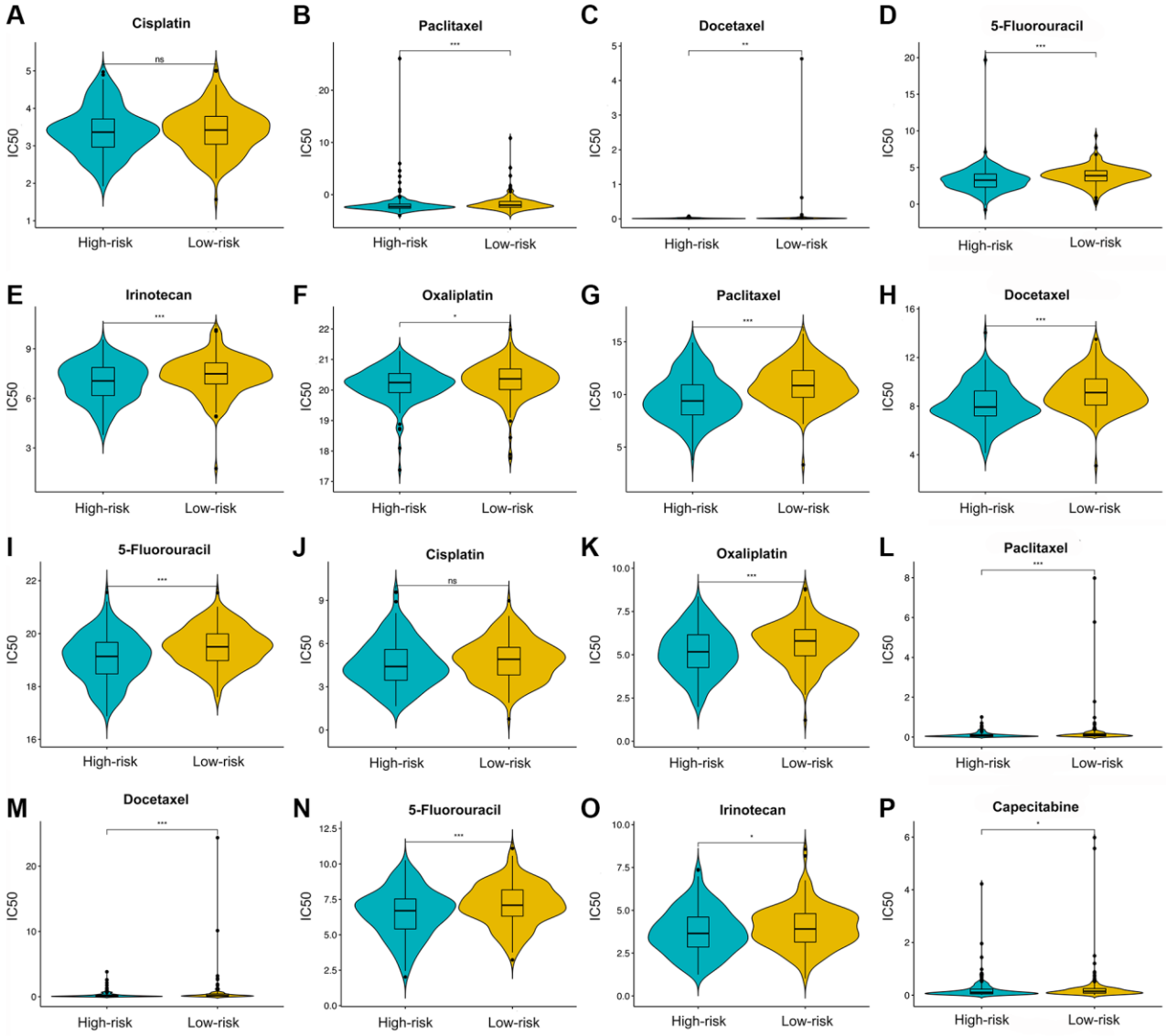

Figure 10. Chemotherapy drugs' sensitivity of the high- versus low-risk group. Differential analysis of IC50 for chemotherapy drugs in CGP (**A–E**), CTRP (**F–I**), and GDSC (**J–P**) databases.

common strategy on which to base clinical management but inevitably has limitations. With the development of genomics and precision medicine, molecular signatures based on gene expression levels have been developed to predict clinical outcomes. Several approaches have been applied for distinguishing the risk-stratified subgroups of GC and helping to formulate individual treatment strategies. Nevertheless, probably due to the high heterogeneity of GC, genes comprising published signatures did not overlap, and more novel signatures are still needed. Immune features have been reported to significantly affect the treatment responses and survival

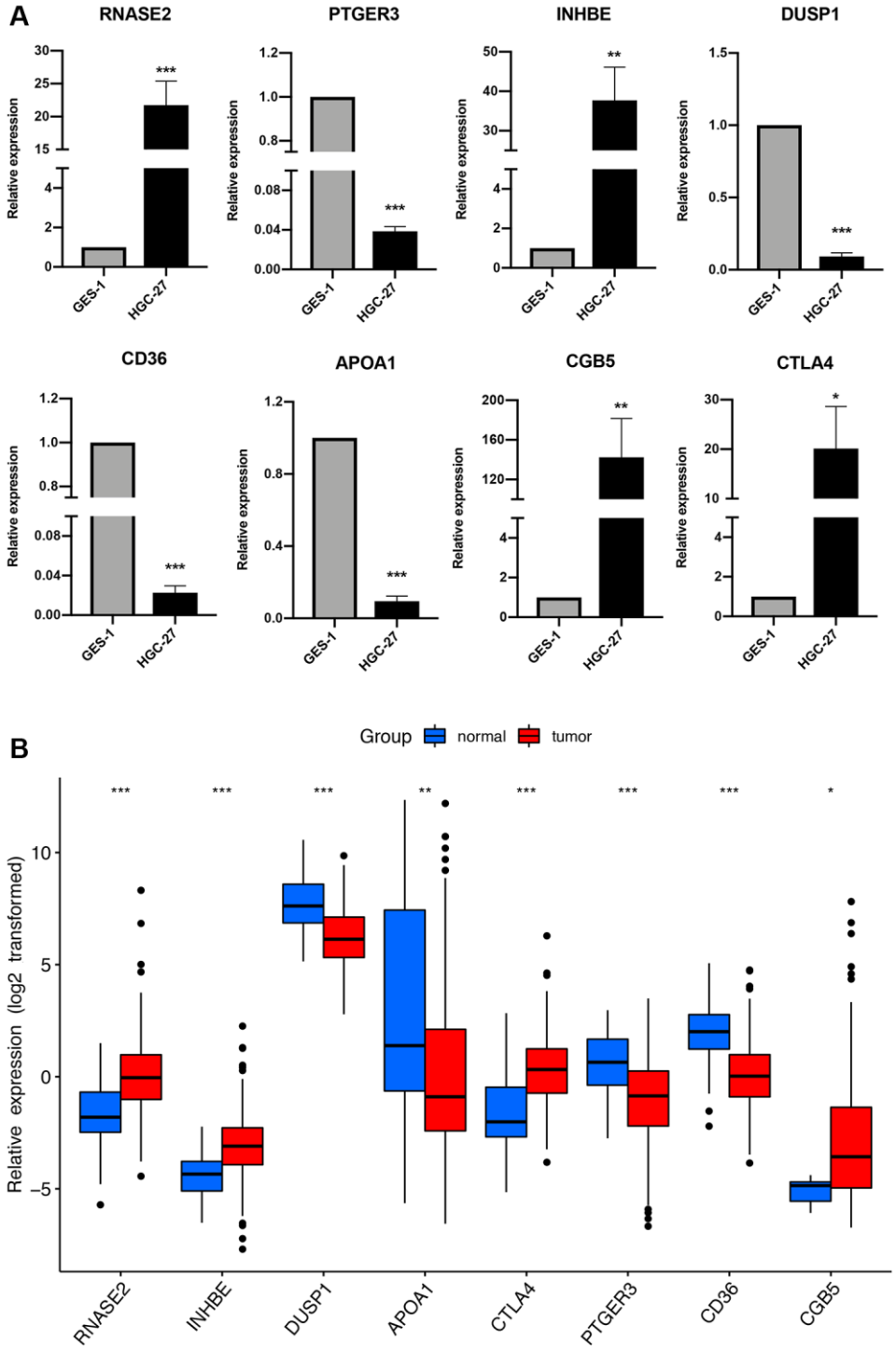

Figure 11. The expression of the immune-related signature in cell lines and TCGA cohort. (**A**) qRT-PCR results of the immune-related signature in GC cell lines (HGC-27) and control cell lines (GES-1). $^{*}P < 0.05$, $^{**}P < 0.01$, $^{***}P < 0.001$. (**B**) The expression of the immune-related signature in TCGA cohort.

of GC patients; thus, several molecular signatures consisting of immune-related genes have been adopted for GC prognosis, and these signatures are usually used to stratify risk groups in patients. However, whether these signatures predict clinical therapeutic responses is still unknown. Moreover, ICIs targeting PD-1, PD-L1, and CTLA4 have been widely utilized and found to significantly prolong survival time in GC patients. Navulizumab in combination with fluorouracil-based and oxaliplatin-based chemotherapy can be a first-line treatment option for patients with advanced HER-2 negative gastric cancer with PD-L1 CPS ≥ 5. The study CheckMmate-649 showed that Navulizumab combined with chemotherapy can significantly improve OS and PFS of GC patients. Pabrolizumab can be used as second-line or follow-up treatment for patients with MSI-H/ dMMR or advanced gastric cancer with high tumor load. The clinical trial revealed that the ORR for these patients was 39.6%, with a 9.9% complete response rate. Besides, dostarlimab-gxly may be used to treat patients with MSI-H/dMMR gastric tumors that have progressed on or after prior treatment, who have no satisfactory alternative treatment options, and who had not previously received a PD-1 or PD-L1 inhibitor. The GARNET trial demonstrated that the ORR was 42%, with a 9% complete response rate. It can be seen that the response rate of GC patients to ICIs treatment is relatively low. There are only a limited group of patients are benefited from the ICIs treatment, thus it remains a challenge to discriminate patients likely to respond well to ICI. Given that, biomarkers predicting patient subpopulations appropriate for ICI treatment warrant intensive investigation.

Previously immune-related gene signatures were mostly established based on the differentially expressed gene sets. Here, we applied the WGCNA analysis to further filter candidate gene markers, which increases the reliability of the final result. After conducting the Cox regression analysis, a final prognostic signature consisting of 8 genes (*RNASE2*, *CGB5*, *INHBE*, *PTGER3*, *CTLA4*, *DUSP1*, *APOA1*, and *CD36*) was constructed. Of these genes, some had previously been reported to play vital roles in cancer. *CD36*, a multi-ligand scavenger receptor expressed on the surface of platelets, adipocytes, hepatocytes, and epithelial cells, was reported to be associated with adverse prognosis and treatment resistance of patients with GC and other solid tumors [23–27]. Additionally, evidence indicated that *CD36* can promote GC cell migration and invasion by inducing c-Myc-dependent DEK transcription, GSK-3β/β-catenin pathway activation, and EMT, suggesting that *CD36* may serve as a novel target in GC [23]. *CTLA4* is one of the most studied immune checkpoints in malignancies, blockade of which has yielded considerable clinical benefits for patients with malignant tumors [28]. Studies showed that *CTLA4* mRNA levels are upregulated in tumor tissues and correlate with a favorable prognosis [29]. *DUSP1* participates in several cellular processes including proliferation, differentiation, and apoptosis. Interestingly, strong expression of *DUSP1* is a favorable prognostic factor in glioma and hepatocellular carcinoma [30, 31]. However, it was also reported to be upregulated in several solid tumors where it facilitated carcinogenesis [32–34], suggesting that the role of *DUSP1* in carcinogenesis could be controversial in different tumors. *CGB5* was reported to be associated with poor prognosis in GC in several bioinformatics studies [35, 36]. Another study suggested that it may promote tumor growth and vascular formation in ovarian cancer via activation of the LHR signal transduction pathway [37]. Previous studies have reported that *PTGER3* is mainly involved in the carcinogenesis of gynecological malignancies [38]. It was found to act as an independent prognostic factor and was associated with poor overall survival in cervical and ovarian cancers [39, 40]. *PTGER3* promotes the tumor cell migration by regulating uPAR expression to affect cervical cancer progression [41]. *APOA1*, a major protein moiety in high-density lipoprotein (HDL) particles, may suppress colorectal tumor progression via regulating the metabolism of intracellular cholesterol [42]. It was found in high amounts in urine from patients with bladder cancer, and utilizing exfoliative urinary cytology in combination with *APOA1* detection increased the sensitivity of diagnosis [43, 44]. Also, studies suggested that *APOA1* might act as an innovative marker in predicting recurrence, development, prognosis, and chemotherapy resistance of some solid tumors [45–47]. There is less data on *INHBE* and *RNASE2* in malignancies, except for some bioinformatics studies reporting their predictive value in cancer prognosis, indicating that more in-depth studies on their biological functions are necessary in the future.

We developed an immune-clinical nomogram consisting of IRS and clinical characteristics (pathological stage and age), which performed well for predicting the prognosis of patients with GC. The DCA curves suggested that combining with the nomogram could yield the most clinical benefit for patients with GC.

The Go enrichment analysis revealed that the activity of cytokines and chemokines, migration of various inflammatory cells, and immune inflammatory responses were significantly enriched in gastric cancer. Previous study revealed that inflammation is a critical component of tumor progression. The inflammatory cells could orchestrate the tumor microenvironment

and participant in the neoplastic process, fostering proliferation, survival and migration [48]. Furthermore, the KEGG analysis showed that the DE-IRGs were enriched in multiple cytokine-related signaling pathways such as cytokine-cytokine receptor interaction, chemokine signaling pathway, viral protein interaction with cytokine and cytokine receptor. Previous studies have shown that cytokines can promote or inhibit tumor growth and invasiveness through multiple pathways, thereby affecting gastric cancer progression [49, 50]. Besides, the inflammation-related pathway such as NF-κB also had significant enrichment. Study demonstrated that the activation of NF-κB signaling has been identified as regulating several sporadic and inflammation-associated gastrointestinal tract malignancies [51]. Summarily, the above results suggest that cytokine activation and immune inflammation have an important role in the development of gastric cancer.

The results suggested that the TMB was generally higher in the LRG. The higher the TMB, the more DNA mutations exist and more candidate peptides generated, leading to a greater likelihood of neoantigens being identified by the immune system [52]. Accumulating studies indicate that the TMB is a potential biomarker for immunotherapy response and prognosis in solid tumors [52, 53]. Interestingly, a high TMB did suggested a favorable prognosis for GC patients according to our results. In keeping with the TMB level in distinct risk subgroups, the LRG presented with a greater genetic mutation frequency, suggesting higher levels of tumor heterogeneity. In particular, it was observed that the LRG had a significantly higher frequency of *TTN* mutation. Some studies reported that *TTN* mutation was associated with increased TMB and related to high immunogenicity. Consequently, the patients with mutated *TTN* exhibited a favorable objective response to ICI treatment and longer progression-free survival or overall survival than those with wild-type status [54, 55].

In addition to tumor cells, nontumor cells such as stromal cells and immune cells are present in the GC TME, which decrease tumor purity. The present study revealed a higher proportion of stromal cells as well as lower tumor purity in the HRG. It has been reported that TME-related stromal cells can positively regulate tumor growth and impair host immune responses, and that low tumor purity is associated with an unfavorable prognosis and an immune-evasion phenotype. This suggests that stromal changes in the development of GC might be deleterious [56, 57]. As a critical component of the TME, the distribution of immune cells also varies across risk groups. As the main effector cells, CD8+ T cells play an important role in host defense against cancer. The current study showed that tumors from the LRG had a higher CD8+ T cells content, and that more infiltration of CD8+ T cells correlated with a better prognosis for patients with GC. This is consistent with a high infiltration of CD8+ T cells enhancing the host's antitumor defense, thereby improving the survival outcomes of GC patients. Activated CD4+ memory T cells and follicular T-helper cells were also copious in the LRG. These cells are likely to bolster the maintenance of a protective immune response against tumor-related antigens, associated with a more favorable prognosis for GC patients in the LRG. Macrophages are an essential component of innate immunity, playing an important role in cancer development and metastasis. Proinflammatory M1 macrophages can phagocytose tumor cells, while anti-inflammatory M2 macrophages promote tumor growth and invasion [58]. This may explain why M1 macrophages were enriched in the LRG while M2 macrophages were clustered in the HRG. Accumulating studies are showing that eosinophils, neutrophils, and monocytes all have disparate effects on cancer progression, encompassing both pro- and anti-tumorigenic roles [59–61]. In the present study, these three immune cell types were more bountiful in the LRG, indicating that they might contribute to the tumor invasion and angiogenesis thereby playing a role in promoting cancer.

Moreover, CCRs can influence the proliferation, invasion, and metastasis of cancer cells and have potential for future immunotherapeutic exploitation [62]. DCs can aid cancer growth and development by facilitating immune tolerance [63]. Mast cells are increased in GC and have been correlated with angiogenesis, and lymph metastasis [64]. The aforesaid immune-related pathways were centered in the HRG, associated with the poor prognosis of GC. Inflammation assists in the proliferation and survival of malignant cells, and stimulates angiogenesis and metastasis, thereby driving tumor initiation, growth, and progression [65]. Inflammation-promoting terms were enriched in the LRG, which might weaken the protective effect. One study pointed out that the primary response to anti-CTLA-4 requires MHC class I expression [66]. In the current study, MHC class I was enriched in the LRG, reflecting a better immunotherapeutic response for the LRG.

Furthermore, we explored the association between IRS and therapeutic responses. ICI treatment has been widely applied for GC, but so far the response rate is relatively low (10–26%) [67]. The present study suggested that TIDE score was lower but the TMB and expression of PD-L1 were higher in LRG. Also, the IRS effectively distinguish patients in the IMvigor210 cohort who benefit from immunotherapy. The

aforementioned results implied that patients with GC in LRG might benefit from immunotherapy, so the IRS may have great potential for predicting immunotherapy responsiveness.

Currently, patients with GC still need to receive systematic chemotherapy [68]. Our results suggest that LRG were more susceptive to conventional chemotherapy drugs such as cisplatin, oxaliplatin, docetaxel, paclitaxel, 5-FU, capecitabine, and irinotecan. On the one hand, docetaxel, paclitaxel, irinotecan, and 5-FU are cell cycle-specific drugs. Paclitaxel or docetaxel can stabilize microtubules and impede the mitosis of cancer cells, thereby effectively preventing their proliferation and mediating anti-cancer effects. Irinotecan inhibits topoisomerase 1 and induces DNA single-strand damage, thus blocking DNA replication and affect the cell cycle. 5-FU is an antimetabolite chemotherapeutic drug that inhibits tumor cell proliferation by affecting nucleic acid synthesis. On the other hand, cisplatin and oxaliplatin, cell-cycle-nonspecific drugs, are not affected by the cell cycle phase and kill rapidly dividing cancer cells via disrupting DNA structure. As mentioned above, the LRG shows a considerable enrichment of the proliferation- and metabolism-related pathways such as cell cycle, DNA replication, and pyrimidine metabolism, which might account for their higher sensitivity to chemotherapeutic drugs.

In brief, we established an IRS which had good predictive performance for prognosis of patients with GC. Patients in the HRG had poor prognosis, more enrichment of oncogenic pathways, low TMB and mutation frequency, more basic immune cells, low expression of immune checkpoints, poor response to immunotherapy, and low sensitivity to common chemotherapeutic drugs. Reciprocally, patients in the LRG had a more favorable prognosis, more enrichment of proliferation pathways, high TMB and mutation frequency, more CD8+ T cells, high expression of immune checkpoints, positive responses to immunotherapy, and high sensitivity to the chemo-therapeutic agents. A nomogram was constructed which appeared to possess great capability for predicting GC patients' survival, the application of which might yield more clinical benefit.

The concept of the IRS has been reported before. The strength of the present study is that we developed a robust IRS using TCGA database and further validated it on an external dataset to ensure the confirmability of the analysis results. Simultaneously, we validated the expression differences of prognostic signatures using PCR, and the results were in good agreement with the bioinformatic analysis, indicating that the results of this study have good verifiability. Furthermore, we investigated the TMB, TME, and immune cell infiltration, and analyzed the response to ICIs as well as sensitivity to chemotherapeutic drugs, which offers a perspective for understanding the specific immune characteristics underlying the IRS and may be vital for GC patients. Regardless of the strengths, our study inevitably has several limitations as well. First, data on clinical characteristics such as Her-2 expression, microsatellite instability, chemotherapy and immunotherapy are insufficient in the TCGA database, yet this information might be necessary for perfecting the nomogram. Second, further functional experiments on the IRS are required to validate our silico results. Finally, clinical responses to ICIs and sensitivity to chemotherapeutic drugs should be further verified in clinical cohorts. In summary, the subsequent validation in a large clinical cohort and the use of experiments to validate the molecular function of the prognostic signature will also be the focus of our future research.

In conclusion, this study underlines the importance of IRGs in GC prognosis and establishes an immune-related prognostic signature, which is expected to improve the prediction of GC patient survival together with well-defined TNM staging. Additionally, the clinical outcome, genetic mutations, immune cell infiltration, immunotherapy response, and chemotherapeutic drug sensitivity underlying the signature were also identified. These results lay the foundation for comprehending the role of IRGs and illustrate the underlying clinical implications of IRGs in GC.

Abbreviations

GC: gastric cancer; IRGs: immune-related genes; IRS: immune-related signature; LRG: low-risk group; HRG: high-risk group; TCGA: the cancer genome atlas; GEO: gene expression omnibus; ICI: immune checkpoint inhibitor; TME: the tumor microenvironment; DEGA: differentially expressed gene analysis; DE: differentially expressed; WGCNA: weighted gene co-expression network analysis; GO: gene ontology; KEGG: kyoto genome encyclopedia; GSEA: gene set enrichment analysis; TMB: tumor mutation burden; TIDE: tumor immune dysfunction and exclusion; CGP: cancer genome project; GDSC: genomics of drug sensitivity in cancer; CTRP: cancer therapeutics portal; IC50: half-maximal inhibitory concentrations; HR: hazard ratio; CI: confidence intervals.

AUTHOR CONTRIBUTIONS

JH S designed this study; JR S, CF K, XK Q, AT S, and KP Z collected and assembled the data; JR S, CF K, and XK Q conducted the data analysis and interpretation; JR S and CF K conducted the experiments. JR S drafted

this manuscript; JH S revised the manuscript; All the authors read and approved the final manuscript.

ACKNOWLEDGMENTS

The authors would like to express their gratitude to EditSprings (https://www.editsprings.cn) for the expert linguistic services provided.

CONFLICTS OF INTEREST

The authors declare no conflicts of interest related to this study.

FUNDING

This study was supported by the National Natural Science Foundation of China (Grant No. 81660772).

REFERENCES

1. Sung H, Ferlay J, Siegel RL, Laversanne M, Soerjomataram I, Jemal A, Bray F. Global Cancer Statistics 2020: GLOBOCAN Estimates of Incidence and Mortality Worldwide for 36 Cancers in 185 Countries. CA Cancer J Clin. 2021; 71:209–49. https://doi.org/10.3322/caac.21660 PMID:33538338

2. Katai H, Ishikawa T, Akazawa K, Isobe Y, Miyashiro I, Oda I, Tsujitani S, Ono H, Tanabe S, Fukagawa T, Nunobe S, Kakeji Y, Nashimoto A, and Registration Committee of the Japanese Gastric Cancer Association. Five-year survival analysis of surgically resected gastric cancer cases in Japan: a retrospective analysis of more than 100,000 patients from the nationwide registry of the Japanese Gastric Cancer Association (2001-2007). Gastric Cancer. 2018; 21:144–54. https://doi.org/10.1007/s10120-017-0716-7 PMID:28417260

3. Wu T, Dai Y. Tumor microenvironment and therapeutic response. Cancer Lett. 2017; 387:61–8. https://doi.org/10.1016/j.canlet.2016.01.043 PMID:26845449

4. Liu YT, Sun ZJ. Turning cold tumors into hot tumors by improving T-cell infiltration. Theranostics. 2021; 11:5365–86. https://doi.org/10.7150/thno.58390 PMID:33859752

5. Peng LS, Zhuang Y, Shi Y, Zhao YL, Wang TT, Chen N, Cheng P, Liu T, Liu XF, Zhang JY, Zuo QF, Mao XH, Guo G, et al. Increased tumor-infiltrating CD8(+)Foxp3(+) T lymphocytes are associated with tumor progression in human gastric cancer. Cancer Immunol Immunother. 2012; 61:2183–92. https://doi.org/10.1007/s00262-012-1277-6 PMID:22729557

6. Chen T, Yang C, Dou R, Xiong B. Identification of a novel 10 immune-related genes signature as a prognostic biomarker panel for gastric cancer. Cancer Med. 2021; 10:6546–60. https://doi.org/10.1002/cam4.4180 PMID:34382341

7. Zhao E, Zhou C, Chen S. A signature of 14 immune-related gene pairs predicts overall survival in gastric cancer. Clin Transl Oncol. 2021; 23:265–74. https://doi.org/10.1007/s12094-020-02414-7 PMID:32519178

8. Huo J, Wu L, Zang Y. Development and Validation of a Robust Immune-Related Prognostic Signature for Gastric Cancer. J Immunol Res. 2021; 2021:5554342. https://doi.org/10.1155/2021/5554342 PMID:34007851

9. Mao C, Ma L, Huang Y, Yang X, Huang H, Cai W, Sitrakiniaina A, Gu R, Xue X, Shen X. Immunogenomic Landscape and Immune-Related Gene-Based Prognostic Signature in Asian Gastric Cancer. Front Oncol. 2021; 11:750768. https://doi.org/10.3389/fonc.2021.750768 PMID:34804939

10. Wagner GP, Kin K, Lynch VJ. Measurement of mRNA abundance using RNA-seq data: RPKM measure is inconsistent among samples. Theory Biosci. 2012; 131:281–5. https://doi.org/10.1007/s12064-012-0162-3 PMID:22872506

11. Leek JT, Johnson WE, Parker HS, Jaffe AE, Storey JD. The sva package for removing batch effects and other unwanted variation in high-throughput experiments. Bioinformatics. 2012; 28:882–3. https://doi.org/10.1093/bioinformatics/bts034 PMID:22257669

12. Langfelder P, Horvath S. WGCNA: an R package for weighted correlation network analysis. BMC Bioinformatics. 2008; 9:559. https://doi.org/10.1186/1471-2105-9-559 PMID:19114008

13. Subramanian A, Tamayo P, Mootha VK, Mukherjee S, Ebert BL, Gillette MA, Paulovich A, Pomeroy SL, Golub TR, Lander ES, Mesirov JP. Gene set enrichment analysis: a knowledge-based approach for interpreting genome-wide expression profiles. Proc Natl Acad Sci U S A. 2005; 102:15545–50. https://doi.org/10.1073/pnas.0506580102 PMID:16199517

14. Yoshihara K, Shahmoradgoli M, Martínez E, Vegesna R, Kim H, Torres-Garcia W, Treviño V, Shen H, Laird PW, Levine DA, Carter SL, Getz G, Stemke-Hale K, et al. Inferring tumour purity and stromal and immune cell admixture from expression data. Nat Commun. 2013; 4:2612. https://doi.org/10.1038/ncomms3612 PMID:24113773

15. Newman AM, Liu CL, Green MR, Gentles AJ, Feng W, Xu Y, Hoang CD, Diehn M, Alizadeh AA. Robust enumeration of cell subsets from tissue expression profiles. Nat Methods. 2015; 12:453–7. https://doi.org/10.1038/nmeth.3337 PMID:25822800

16. Li T, Fu J, Zeng Z, Cohen D, Li J, Chen Q, Li B, Liu XS. TIMER2.0 for analysis of tumor-infiltrating immune cells. Nucleic Acids Res. 2020; 48:W509–14. https://doi.org/10.1093/nar/gkaa407 PMID:32442275

17. Aran D, Hu Z, Butte AJ. xCell: digitally portraying the tissue cellular heterogeneity landscape. Genome Biol. 2017; 18:220. https://doi.org/10.1186/s13059-017-1349-1 PMID:29141660

18. Racle J, Gfeller D. EPIC: A Tool to Estimate the Proportions of Different Cell Types from Bulk Gene Expression Data. Methods Mol Biol. 2020; 2120:233–48. https://doi.org/10.1007/978-1-0716-0327-7_17 PMID:32124324

19. Plattner C, Finotello F, Rieder D. Deconvoluting tumor-infiltrating immune cells from RNA-seq data using quanTIseq. Methods Enzymol. 2020; 636:261–85. https://doi.org/10.1016/bs.mie.2019.05.056 PMID:32178821

20. Jiang P, Gu S, Pan D, Fu J, Sahu A, Hu X, Li Z, Traugh N, Bu X, Li B, Liu J, Freeman GJ, Brown MA, et al. Signatures of T cell dysfunction and exclusion predict cancer immunotherapy response. Nat Med. 2018; 24:1550–8. https://doi.org/10.1038/s41591-018-0136-1 PMID:30127393

21. Ding MQ, Chen L, Cooper GF, Young JD, Lu X. Precision Oncology beyond Targeted Therapy: Combining Omics Data with Machine Learning Matches the Majority of Cancer Cells to Effective Therapeutics. Mol Cancer Res. 2018; 16:269–78. https://doi.org/10.1158/1541-7786.MCR-17-0378 PMID:29133589

22. Thul PJ, Lindskog C. The human protein atlas: A spatial map of the human proteome. Protein Sci. 2018; 27:233–44. https://doi.org/10.1002/pro.3307 PMID:28940711

23. Wang J, Wen T, Li Z, Che X, Gong L, Jiao Z, Qu X, Liu Y. CD36 upregulates DEK transcription and promotes cell migration and invasion via GSK-3β/β-catenin-mediated epithelial-to-mesenchymal transition in gastric cancer. Aging (Albany NY). 2020; 13:1883–97. https://doi.org/10.18632/aging.103985 PMID:33232276

24. Pan J, Fan Z, Wang Z, Dai Q, Xiang Z, Yuan F, Yan M, Zhu Z, Liu B, Li C. CD36 mediates palmitate acid-induced metastasis of gastric cancer via AKT/GSK-3β/β-catenin pathway. J Exp Clin Cancer Res. 2019; 38:52. https://doi.org/10.1186/s13046-019-1049-7 PMID:30717785

25. Deng M, Cai X, Long L, Xie L, Ma H, Zhou Y, Liu S, Zeng C. CD36 promotes the epithelial-mesenchymal transition and metastasis in cervical cancer by interacting with TGF-β. J Transl Med. 2019; 17:352. https://doi.org/10.1186/s12967-019-2098-6 PMID:31655604

26. Xu WH, Qu YY, Wang J, Wang HK, Wan FN, Zhao JY, Zhang HL, Ye DW. Elevated CD36 expression correlates with increased visceral adipose tissue and predicts poor prognosis in ccRCC patients. J Cancer. 2019; 10:4522–31. https://doi.org/10.7150/jca.30989 PMID:31528216

27. Kubo M, Gotoh K, Eguchi H, Kobayashi S, Iwagami Y, Tomimaru Y, Akita H, Asaoka T, Noda T, Takeda Y, Tanemura M, Mori M, Doki Y. Impact of CD36 on Chemoresistance in Pancreatic Ductal Adenocarcinoma. Ann Surg Oncol. 2020; 27:610–9. https://doi.org/10.1245/s10434-019-07927-2 PMID:31605325

28. Pardoll DM. The blockade of immune checkpoints in cancer immunotherapy. Nat Rev Cancer. 2012; 12:252–64. https://doi.org/10.1038/nrc3239 PMID:22437870

29. Saleh R, Taha RZ, Toor SM, Sasidharan Nair V, Murshed K, Khawar M, Al-Dhaheri M, Petkar MA, Abu Nada M, Elkord E. Expression of immune checkpoints and T cell exhaustion markers in early and advanced stages of colorectal cancer. Cancer Immunol Immunother. 2020; 69:1989–99. https://doi.org/10.1007/s00262-020-02593-w PMID:32393998

30. Arrizabalaga O, Moreno-Cugnon L, Auzmendi-Iriarte J, Aldaz P, Ibanez de Caceres I, Garros-Regulez L,

Moncho-Amor V, Torres-Bayona S, Pernía O, Pintado-Berninches L, Carrasco-Ramirez P, Cortes-Sempere M, Rosas R, et al. High expression of MKP1/DUSP1 counteracts glioma stem cell activity and mediates HDAC inhibitor response. Oncogenesis. 2017; 6:401. https://doi.org/10.1038/s41389-017-0003-9 PMID:29284798

31. Calvisi DF, Pinna F, Meloni F, Ladu S, Pellegrino R, Sini M, Daino L, Simile MM, De Miglio MR, Virdis P, Frau M, Tomasi ML, Seddaiu MA, et al. Dual-specificity phosphatase 1 ubiquitination in extracellular signal-regulated kinase-mediated control of growth in human hepatocellular carcinoma. Cancer Res. 2008; 68:4192–200. https://doi.org/10.1158/0008-5472.CAN-07-6157 PMID:18519678

32. Lopes LJS, Tesser-Gamba F, Petrilli AS, de Seixas Alves MT, Garcia-Filho RJ, Toledo SRC. MAPK pathways regulation by DUSP1 in the development of osteosarcoma: Potential markers and therapeutic targets. Mol Carcinog. 2017; 56:1630–41. https://doi.org/10.1002/mc.22619 PMID:28112450

33. Fan MK, Zhang GC, Chen W, Qi LL, Xie MF, Zhang YY, Wang L, Zhang Q. Siglec-15 Promotes Tumor Progression in Osteosarcoma via DUSP1/MAPK Pathway. Front Oncol. 2021; 11:710689. https://doi.org/10.3389/fonc.2021.710689 PMID:34336699

34. Vicent S, Garayoa M, López-Picazo JM, Lozano MD, Toledo G, Thunnissen FB, Manzano RG, Montuenga LM. Mitogen-activated protein kinase phosphatase-1 is overexpressed in non-small cell lung cancer and is an independent predictor of outcome in patients. Clin Cancer Res. 2004; 10:3639–49. https://doi.org/10.1158/1078-0432.CCR-03-0771 PMID:15173070

35. Yang Y, Shi Y, Hou Y, Lu Y, Yang J. CGB5 expression is independently associated with poor overall survival and recurrence-free survival in patients with advanced gastric cancer. Cancer Med. 2018; 7:716–25. https://doi.org/10.1002/cam4.1364 PMID:29473345

36. Qiu XT, Song YC, Liu J, Wang ZM, Niu X, He J. Identification of an immune-related gene-based signature to predict prognosis of patients with gastric cancer. World J Gastrointest Oncol. 2020; 12:857–76. https://doi.org/10.4251/wjgo.v12.i8.857 PMID:32879664

37. Gao S, Fan C, Huang H, Zhu C, Su M, Zhang Y. Effects of HCG on human epithelial ovarian cancer vasculogenic mimicry formation *in vivo*. Oncol Lett. 2016; 12:459–66. https://doi.org/10.3892/ol.2016.4630 PMID:27347165

38. Ye Y, Wang X, Jeschke U, von Schönfeldt V. COX-2-PGE_2-EPs in gynecological cancers. Arch Gynecol Obstet. 2020; 301:1365–75. https://doi.org/10.1007/s00404-020-05559-6 PMID:32363546

39. Heidegger H, Dietlmeier S, Ye Y, Kuhn C, Vattai A, Aberl C, Jeschke U, Mahner S, Kost B. The Prostaglandin EP3 Receptor Is an Independent Negative Prognostic Factor for Cervical Cancer Patients. Int J Mol Sci. 2017; 18:1571. https://doi.org/10.3390/ijms18071571 PMID:28753926

40. Millstein J, Budden T, Goode EL, Anglesio MS, Talhouk A, Intermaggio MP, Leong HS, Chen S, Elatre W, Gilks B, Nazeran T, Volchek M, Bentley RC, et al, and AOCS Group. Prognostic gene expression signature for high-grade serous ovarian cancer. Ann Oncol. 2020; 31:1240–50. https://doi.org/10.1016/j.annonc.2020.05.019 PMID:32473302

41. Ye Y, Peng L, Vattai A, Deuster E, Kuhn C, Dannecker C, Mahner S, Jeschke U, von Schönfeldt V, Heidegger HH. Prostaglandin E2 receptor 3 (EP3) signaling promotes migration of cervical cancer via urokinase-type plasminogen activator receptor (uPAR). J Cancer Res Clin Oncol. 2020; 146:2189–203. https://doi.org/10.1007/s00432-020-03272-0 PMID:32488496

42. Aguirre-Portolés C, Feliu J, Reglero G, Ramírez de Molina A. ABCA1 overexpression worsens colorectal cancer prognosis by facilitating tumour growth and caveolin-1-dependent invasiveness, and these effects can be ameliorated using the BET inhibitor apabetalone. Mol Oncol. 2018; 12:1735–52. https://doi.org/10.1002/1878-0261.12367 PMID:30098223

43. Li H, Li C, Wu H, Zhang T, Wang J, Wang S, Chang J. Identification of Apo-A1 as a biomarker for early diagnosis of bladder transitional cell carcinoma. Proteome Sci. 2011; 9:21. https://doi.org/10.1186/1477-5956-9-21 PMID:21496341

44. Li C, Li H, Zhang T, Li J, Liu L, Chang J. Discovery of Apo-A1 as a potential bladder cancer biomarker by urine proteomics and analysis. Biochem Biophys Res Commun. 2014; 446:1047–52. https://doi.org/10.1016/j.bbrc.2014.03.053 PMID:24661883

45. Ni XC, Yi Y, Fu YP, Cai XY, Liu G, Huang JL, Gan W, Xu

J, Qiu SJ. Role of Lipids and Apolipoproteins in Predicting the Prognosis of Hepatocellular Carcinoma After Resection. Onco Targets Ther. 2020; 13:12867–80.
https://doi.org/10.2147/OTT.S279997
PMID:33376344

46. Guo Y, Huang B, Li R, Li J, Tian S, Peng C, Dong W. Low APOA-1 Expression in Hepatocellular Carcinoma Patients Is Associated With DNA Methylation and Poor Overall Survival. Front Genet. 2021; 12:760744.
https://doi.org/10.3389/fgene.2021.760744
PMID:34790226

47. Braoudaki M, Lambrou GI, Vougas K, Karamolegou K, Tsangaris GT, Tzortzatou-Stathopoulou F. Protein biomarkers distinguish between high- and low-risk pediatric acute lymphoblastic leukemia in a tissue specific manner. J Hematol Oncol. 2013; 6:52.
https://doi.org/10.1186/1756-8722-6-52
PMID:23849470

48. Coussens LM, Werb Z. Inflammation and cancer. Nature. 2002; 420:860–7.
https://doi.org/10.1038/nature01322
PMID:12490959

49. Lee DH, Yang Y, Lee SJ, Kim KY, Koo TH, Shin SM, Song KS, Lee YH, Kim YJ, Lee JJ, Choi I, Lee JH. Macrophage inhibitory cytokine-1 induces the invasiveness of gastric cancer cells by up-regulating the urokinase-type plasminogen activator system. Cancer Res. 2003; 63:4648–55.
PMID:12907645

50. Zhou Q, Wu X, Wang X, Yu Z, Pan T, Li Z, Chang X, Jin Z, Li J, Zhu Z, Liu B, Su L. The reciprocal interaction between tumor cells and activated fibroblasts mediated by TNF-α/IL-33/ST2L signaling promotes gastric cancer metastasis. Oncogene. 2020; 39:1414–28.
https://doi.org/10.1038/s41388-019-1078-x
PMID:31659258

51. Merga YJ, O'Hara A, Burkitt MD, Duckworth CA, Probert CS, Campbell BJ, Pritchard DM. Importance of the alternative NF-κB activation pathway in inflammation-associated gastrointestinal carcinogenesis. Am J Physiol Gastrointest Liver Physiol. 2016; 310:G1081–90.
https://doi.org/10.1152/ajpgi.00026.2016
PMID:27102559

52. Jardim DL, Goodman A, de Melo Gagliato D, Kurzrock R. The Challenges of Tumor Mutational Burden as an Immunotherapy Biomarker. Cancer Cell. 2021; 39:154–73.
https://doi.org/10.1016/j.ccell.2020.10.001
PMID:33125859

53. Goodman AM, Kato S, Bazhenova L, Patel SP, Frampton GM, Miller V, Stephens PJ, Daniels GA, Kurzrock R. Tumor Mutational Burden as an Independent Predictor of Response to Immunotherapy in Diverse Cancers. Mol Cancer Ther. 2017; 16:2598–608.
https://doi.org/10.1158/1535-7163.MCT-17-0386
PMID:28835386

54. Jia Q, Wang J, He N, He J, Zhu B. Titin mutation associated with responsiveness to checkpoint blockades in solid tumors. JCI Insight. 2019; 4:127901.
https://doi.org/10.1172/jci.insight.127901
PMID:31092729

55. Xie X, Tang Y, Sheng J, Shu P, Zhu X, Cai X, Zhao C, Wang L, Huang X. *Titin* Mutation Is Associated With Tumor Mutation Burden and Promotes Antitumor Immunity in Lung Squamous Cell Carcinoma. Front Cell Dev Biol. 2021; 9:761758.
https://doi.org/10.3389/fcell.2021.761758
PMID:34746153

56. Gajewski TF, Schreiber H, Fu YX. Innate and adaptive immune cells in the tumor microenvironment. Nat Immunol. 2013; 14:1014–22.
https://doi.org/10.1038/ni.2703
PMID:24048123

57. Gong Z, Zhang J, Guo W. Tumor purity as a prognosis and immunotherapy relevant feature in gastric cancer. Cancer Med. 2020; 9:9052–63.
https://doi.org/10.1002/cam4.3505
PMID:33030278

58. Xia Y, Rao L, Yao H, Wang Z, Ning P, Chen X. Engineering Macrophages for Cancer Immunotherapy and Drug Delivery. Adv Mater. 2020; 32:e2002054.
https://doi.org/10.1002/adma.202002054
PMID:32856350

59. Grisaru-Tal S, Itan M, Klion AD, Munitz A. A new dawn for eosinophils in the tumour microenvironment. Nat Rev Cancer. 2020; 20:594–607.
https://doi.org/10.1038/s41568-020-0283-9
PMID:32678342

60. Mizuno R, Kawada K, Itatani Y, Ogawa R, Kiyasu Y, Sakai Y. The Role of Tumor-Associated Neutrophils in Colorectal Cancer. Int J Mol Sci. 2019; 20:529.
https://doi.org/10.3390/ijms20030529
PMID:30691207

61. Olingy CE, Dinh HQ, Hedrick CC. Monocyte heterogeneity and functions in cancer. J Leukoc Biol. 2019; 106:309–22.
https://doi.org/10.1002/JLB.4RI0818-311R
PMID:30776148

62. Mollica Poeta V, Massara M, Capucetti A, Bonecchi R. Chemokines and Chemokine Receptors: New Targets

for Cancer Immunotherapy. Front Immunol. 2019; 10:379.
https://doi.org/10.3389/fimmu.2019.00379
PMID:30894861

63. DeVito NC, Plebanek MP, Theivanthiran B, Hanks BA. Role of Tumor-Mediated Dendritic Cell Tolerization in Immune Evasion. Front Immunol. 2019; 10:2876.
https://doi.org/10.3389/fimmu.2019.02876
PMID:31921140

64. Sammarco G, Varricchi G, Ferraro V, Ammendola M, De Fazio M, Altomare DF, Luposella M, Maltese L, Currò G, Marone G, Ranieri G, Memeo R. Mast Cells, Angiogenesis and Lymphangiogenesis in Human Gastric Cancer. Int J Mol Sci. 2019; 20:2106.
https://doi.org/10.3390/ijms20092106
PMID:31035644

65. Candido J, Hagemann T. Cancer-related inflammation. J Clin Immunol. 2013 (Suppl 1); 33:S79–84.
https://doi.org/10.1007/s10875-012-9847-0
PMID:23225204

66. Rodig SJ, Gusenleitner D, Jackson DG, Gjini E, Giobbie-Hurder A, Jin C, Chang H, Lovitch SB, Horak C, Weber JS, Weirather JL, Wolchok JD, Postow MA, et al. MHC proteins confer differential sensitivity to CTLA-4 and PD-1 blockade in untreated metastatic melanoma. Sci Transl Med. 2018; 10:eaar3342.
https://doi.org/10.1126/scitranslmed.aar3342
PMID:30021886

67. Muro K, Chung HC, Shankaran V, Geva R, Catenacci D, Gupta S, Eder JP, Golan T, Le DT, Burtness B, McRee AJ, Lin CC, Pathiraja K, et al. Pembrolizumab for patients with PD-L1-positive advanced gastric cancer (KEYNOTE-012): a multicentre, open-label, phase 1b trial. Lancet Oncol. 2016; 17:717–26.
https://doi.org/10.1016/S1470-2045(16)00175-3
PMID:27157491

68. Arai H, Nakajima TE. Recent Developments of Systemic Chemotherapy for Gastric Cancer. Cancers (Basel). 2020; 12:1100.
https://doi.org/10.3390/cancers12051100
PMID:32354119

SUPPLEMENTARY MATERIALS

Supplementary Figures

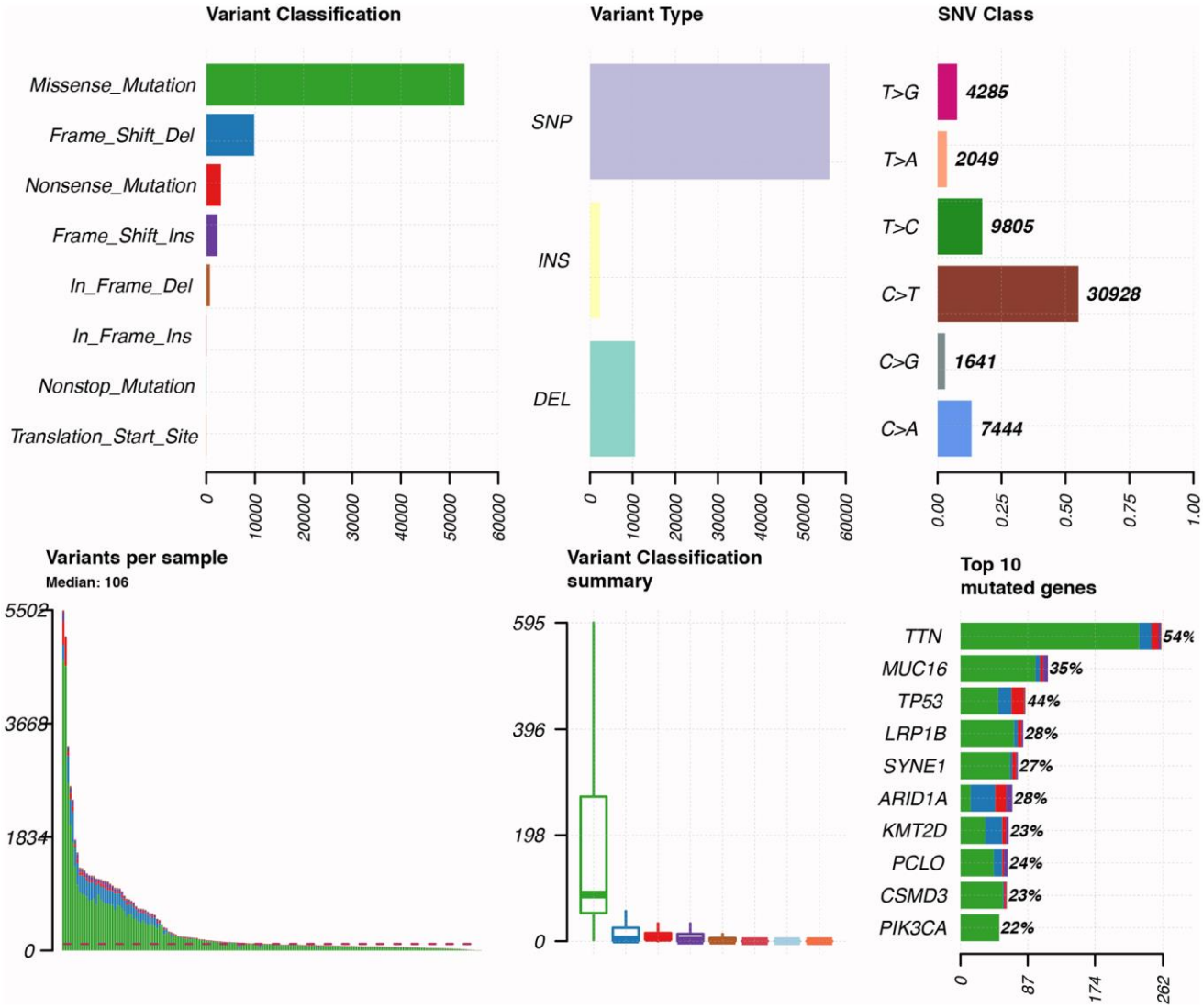

Supplementary Figure 1. Summaries of gene mutation profiles for low-risk group.

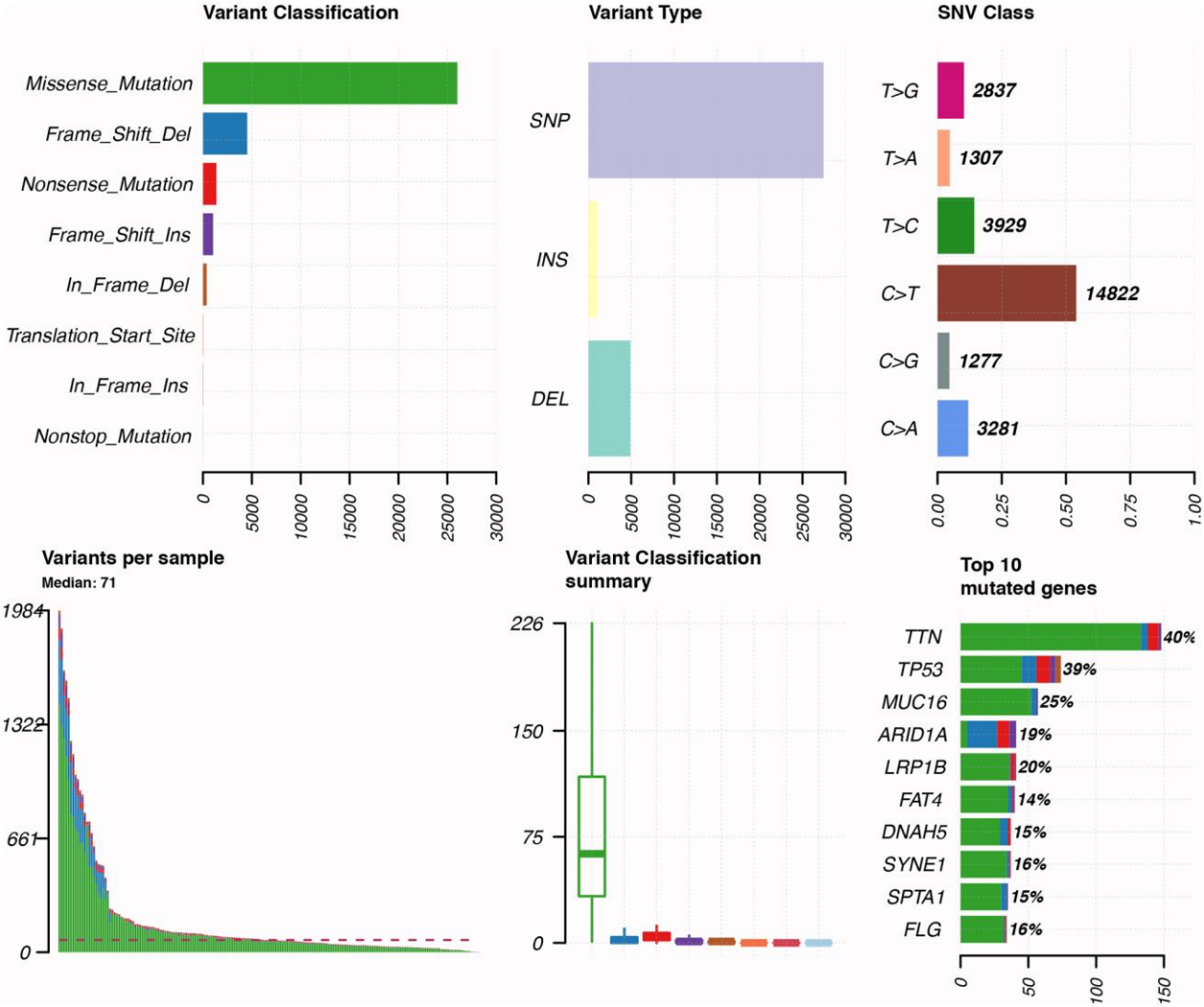

Supplementary Figure 2. Summaries of gene mutation profiles for high-risk group.

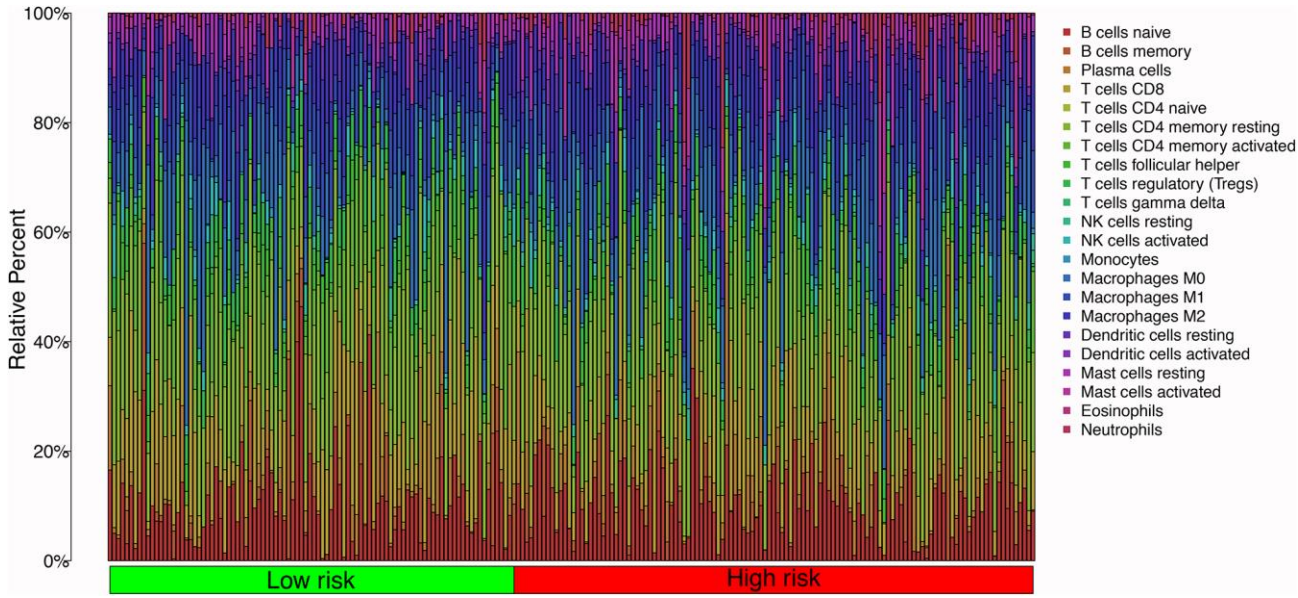

Supplementary Figure 3. The histogram of immune cells' abundance in GC samples.

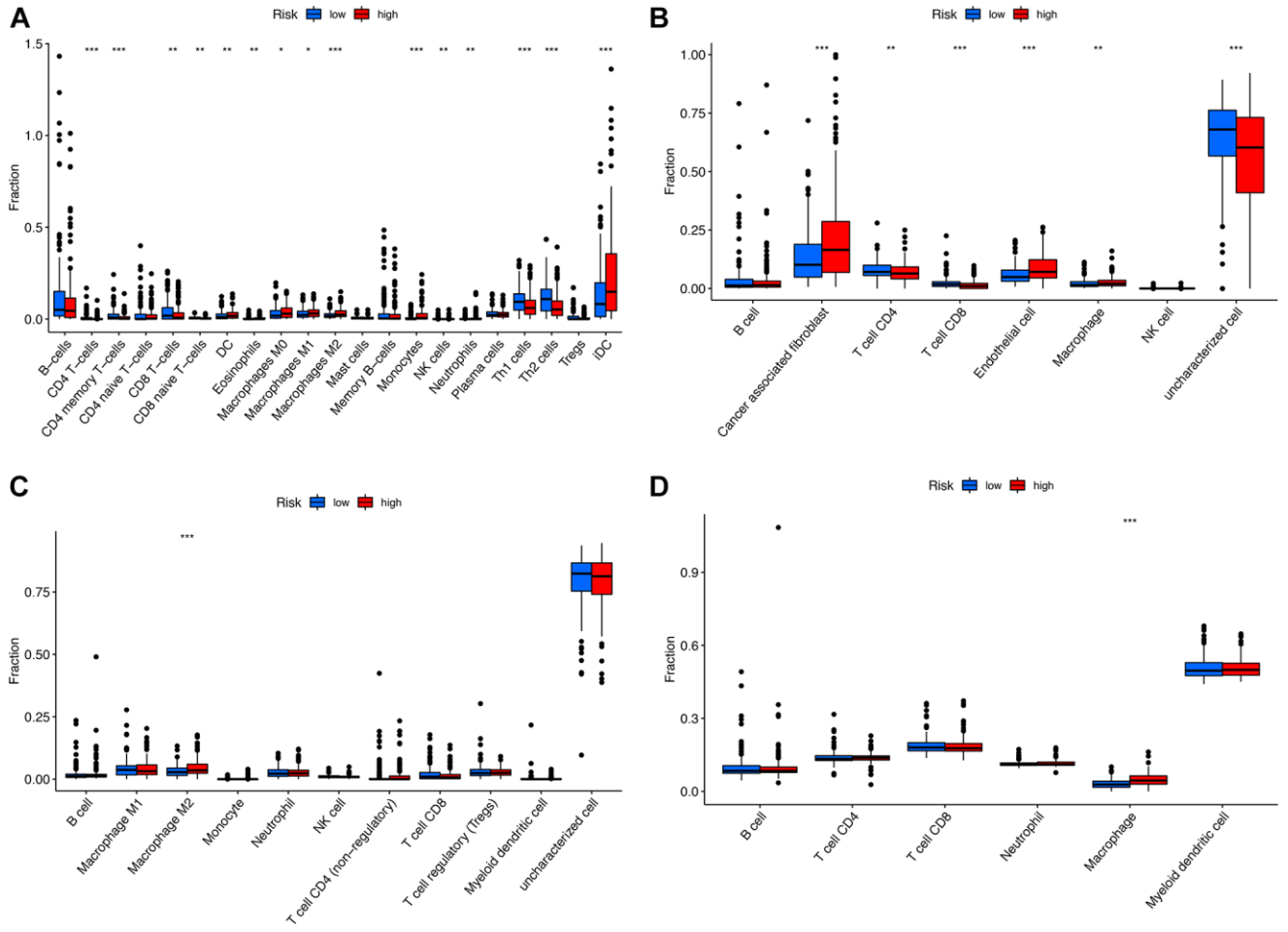

Supplementary Figure 4. The immune cell infiltration in different risk groups analyzed by XCELL (**A**), EPIC (**B**), QUANTISEQ (**C**), and TIMER (**D**).

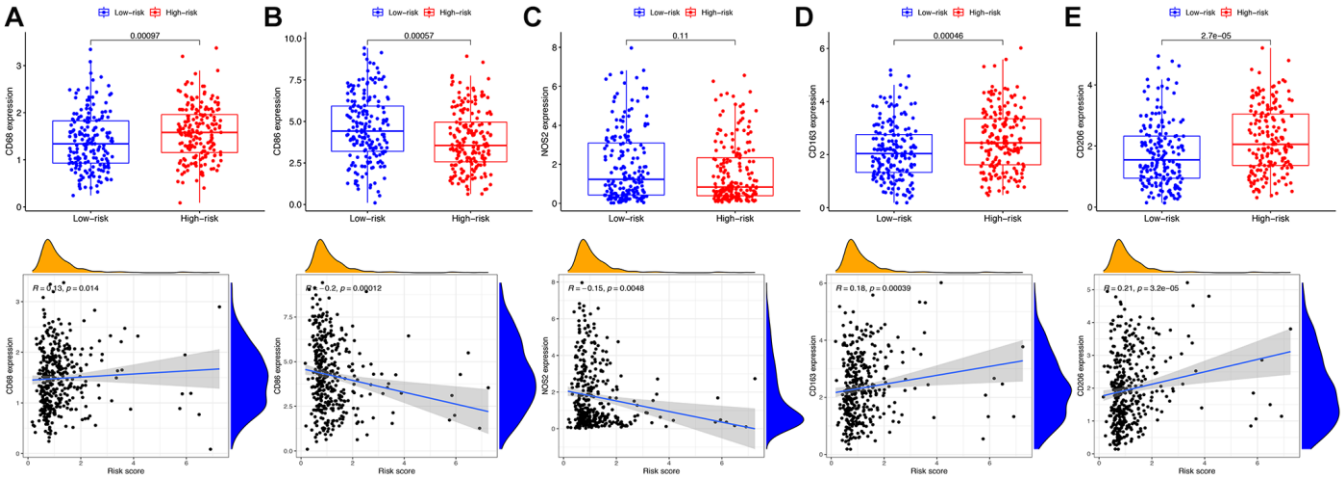

Supplementary Figure 5. The expression of markers for M0 macrophages (**A**), M1 macrophages (**B**, **C**), M2 macrophages (**D**, **E**).

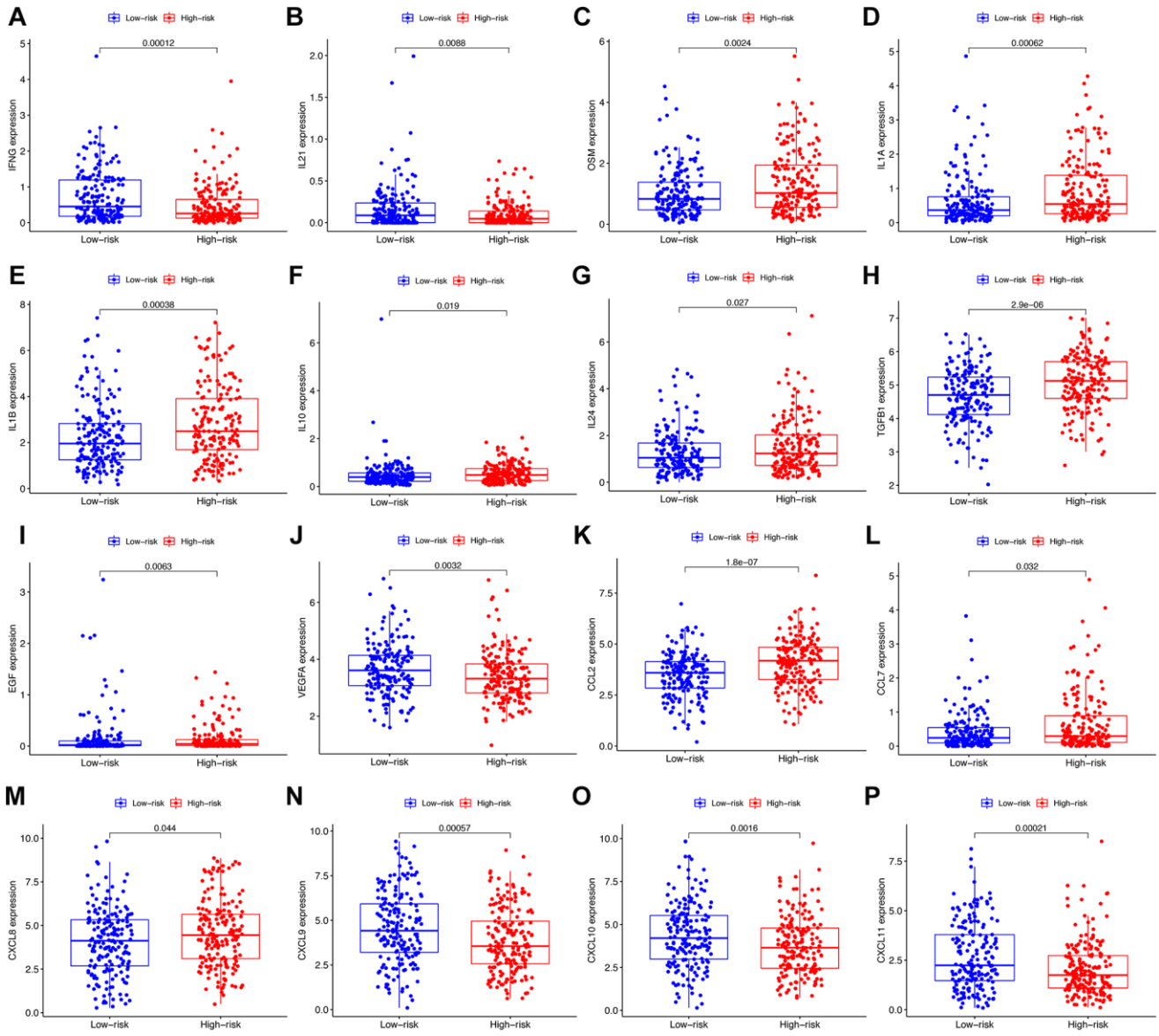

Supplementary Figure 6. The expression of cytokine (**A–J**) and chemokine (**K–P**).

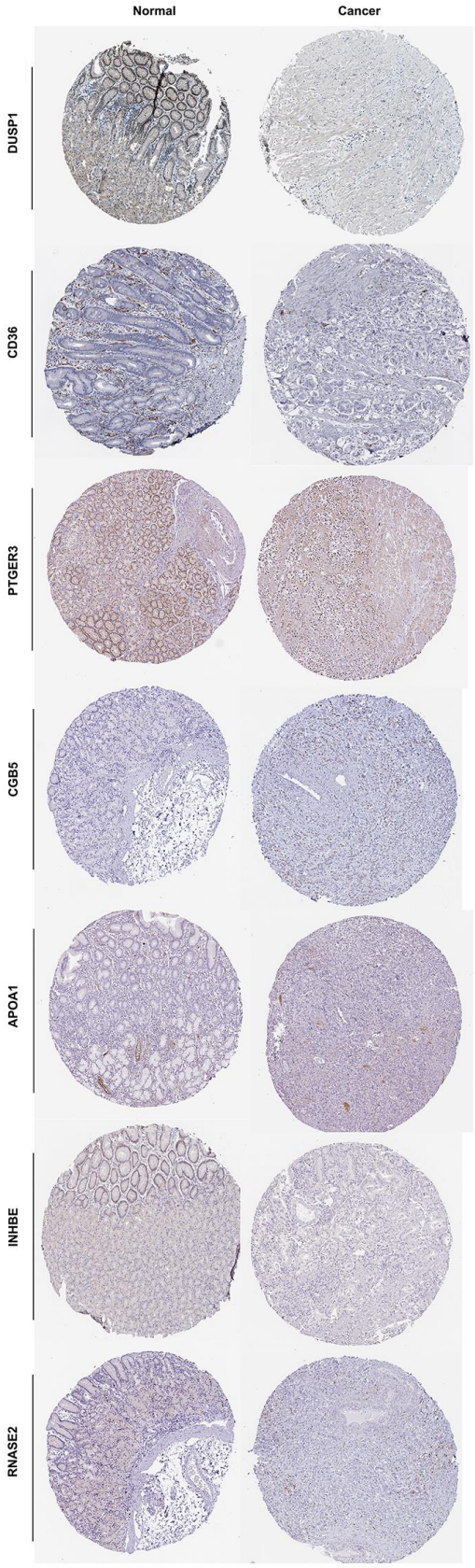

Supplementary Figure 7. The immunohistochemical analysis of the protein expression of the genes in the IRS in the HPA database.

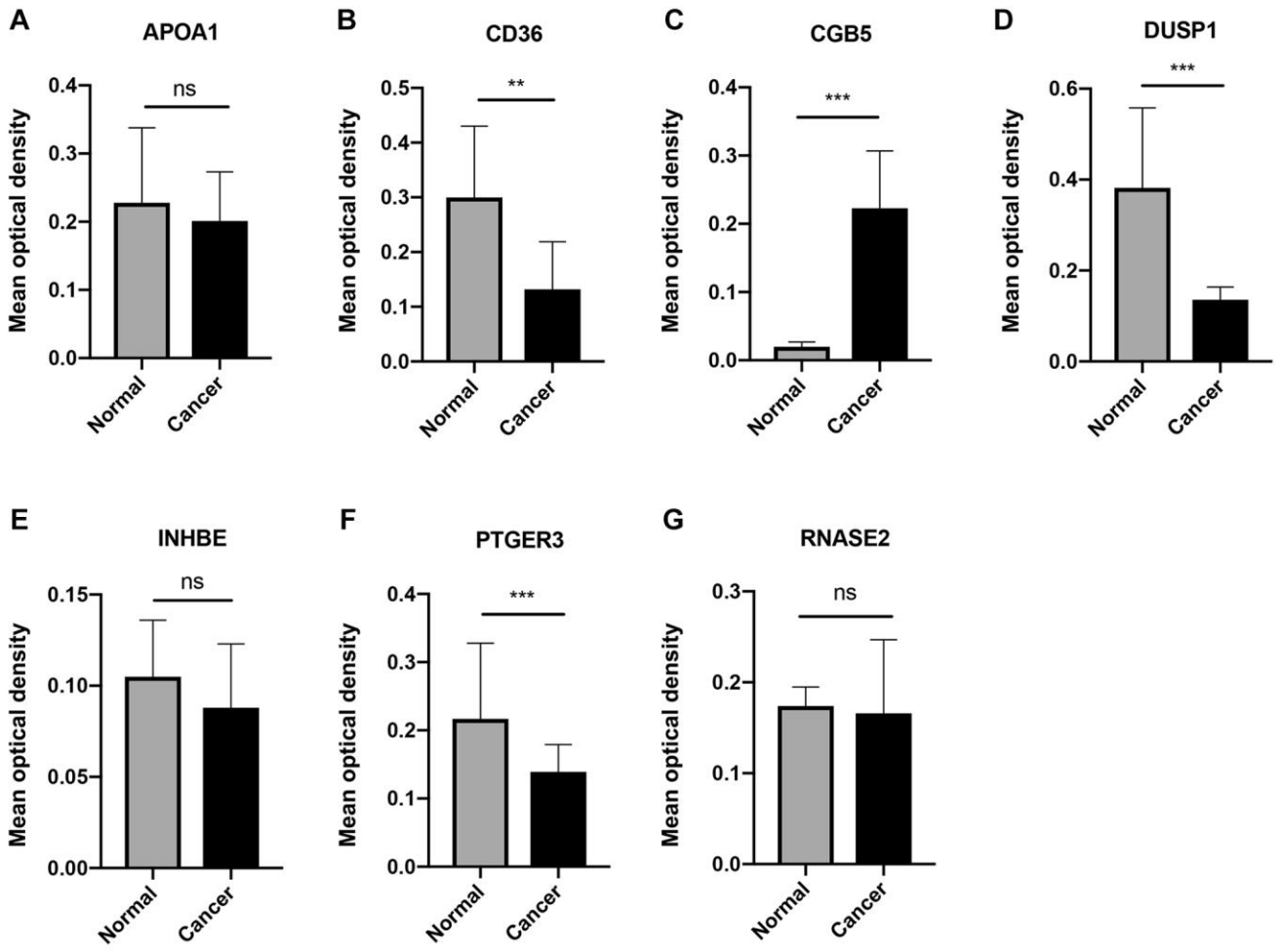

Supplementary Figure 8. The quantitative analysis of immunohistochemical images. The quantitative analysis plots of APOA1 (**A**), CD36 (**B**), CGB5 (**C**), DUSP1 (**D**), INHBE (**E**), PTGER3 (**F**), RNASE2 (**G**). Data are presented as mean ± SD, $^{**}P < 0.01$, $^{***}P < 0.001$, and 'ns' represents no statistical significance.

Supplementary Tables

Please browse Full Text version to see the data of Supplementary Tables 3, 4, 6–11.

Supplementary Table 1. The baseline features of GC patients in TCGA and GEO datasets.

Features	TCGA (*n* = 371)	GSE84437 (*n* = 433)
Age, years (mean ± SD)	65.54 ± 10.55	60.06 ± 11.58
Gender		
Male	230	296
Female	141	137
Tumor grade		
G1	25	–
G2	129	–
G3	209	–
G4	8	–
Pathologic stage		
I–II	173	157
III–IV	198	276
Tumor size		
T1	16	11
T2	70	38
T3	161	92
T4	124	292
Lymph node metastasis		
N0	109	80
N1	115	188
N2	72	132
N3	75	33
Metastasis status		
M0	319	347
M1	52	86

The "–" indicates that the value is not available. Abbreviations: HR: hazard ratio; CI: confidence interval.

Supplementary Table 2. The baseline features of patients in IMvigor210 cohort.

Features	*n* = 348
OS, months (mean ± SD)	10.25 ± 7.65
Survival status	
Alive	232
Dead	116
Gender	
Female	76
Male	272
Tobacco. Use. History	209
Current	35
Never	116
Previous	197
Baseline. ECOG. Score	198
0	134
1	196
2	18
Immune. Phenotype	161
Desert	76
Exclude	134
Inflamed	74
Unknown	64
Binary Response	72
CR/PR	68
SD/PD	230
Unknown	50
Mutation burden per MB (mean ± SD)	10.86 ± 9.57

Abbreviations: OS: overall survival; ECOG: eastern cooperative oncology group; CR: complete remission; PR: partial remission; SD: stable disease; PD: progressive disease.

Supplementary Table 3. Detailed information of the immune-related genes in ImmPort database.

Supplementary Table 4. Detailed information of the immune-related genes in InnateDB database.

Supplementary Table 5. The primers sequences for mRNAs of the immune-related signature.

Gene name	Forward sequence (5′–3′)	Reverse sequence (5′–3′)
GAPDH	TGCACCACCAACTGCTTAGC	ATCGAGTGAAGGACCTGGC
DUSP1	GTACATCAAGTCCATCTGAC	GGTTCTTCTAGGAGTAGACA
APOA1	AGCTTGCTGAAGGTGGAGGT	ATCGAGTGAAGGACCTGGC
CTLA4	CACAAGGCTCAGCTGAACCT	AGGTGCCCGTGCAGATGGAA
PTGER3	AAGGCCACGGCATCTCAGT	TGATCCCCATAAGCTGAATGG
RNASE2	TGATCCCCATAAGCTGAATGG	ACCATGTTTCCCAGTCTCCG
CD36	ACGGGCTGAGCAAGGTTGA	TTCGTTGGGTGGGTAGATGG

CGB5	GCTACTGCCCCACCATGACC	ATGGACTCGAAGCGCACATC
INHBE	AGCCCTTCCTAGAGCTTAAG	GCTGCAGCCACAGGCC

Supplementary Table 6. Differentially expressed genes.

Supplementary Table 7. The immune-related gene list in the ImmPort database.

Supplementary Table 8. The immune-related gene list in the InnateDB database.

Supplementary Table 9. The immune-related genes integrated by two databases.

Supplementary Table 10. Differentially expressed immune-related genes.

Supplementary Table 11. Gene list in turquoise module after WGCNA analysis.

Supplementary Table 12. The prognostic signature identified by multivariate Cox regression analysis.

Gene	HR (CI 95%)	*P*-value	Coefficient
RNASE2	1.32 (1.03–1.68)	0.026	0.28
CGB5	1.29 (1.10–1.52)	0.002	0.26
INHBE	1.65 (0.98–2.79)	0.061	0.50
PTGER3	0.71 (0.44–1.13)	0.145	−0.35
CTLA4	0.71 (0.55–0.93)	0.012	–.034
DUSP1	1.30 (1.07–1.57)	0.008	0.26
APOA1	1.07 (0.99–1.17)	0.092	0.07
CD36	1.26 (1.00–1.60)	0.055	0.23